ORIGINAL RESEARCH

American Society of Plant Biologists | S·E·B SOCIETY FOR EXPERIMENTAL BIOLOGY | WILEY

Cell wall composition and transcriptomics in stem tissues of stinging nettle (*Urtica dioica* L.): Spotlight on a neglected fibre crop

Xuan Xu[1] | Aurélie Backes[1] | Sylvain Legay[1] | Roberto Berni[2,3] | Claudia Faleri[2] | Edoardo Gatti[4] | Jean-Francois Hausman[1] | Giampiero Cai[2] | Gea Guerriero[1]

[1]Environmental Research and Innovation (ERIN) Department, Luxembourg Institute of Science and Technology (LIST), Esch/Alzette, Luxembourg

[2]Department of Life Sciences, University of Siena, Siena, Italy

[3]Trees and Timber Institute-National Research Council of Italy (CNR-IVALSA), Follonica, Italy

[4]Institute of Biometeorology (IBIMET), National Research Council, Bologna, Italy

Correspondence
Gea Guerriero, Luxembourg Institute of Science and Technology (LIST), Environmental Research and Innovation (ERIN) Department, Esch/Alzette L-4362, Luxembourg.
Email: gea.guerriero@list.lu

Present address
Aurélie Backes, Unité de Recherche Résistance Induite et BioProtection des Plantes, UFR Sciences Exactes et Naturelles, SFR Condorcet FR CNRS 3417, Université de Reims-Champagne-Ardenne, Reims Cedex 2, France

Abstract

Stinging nettle (*Urtica dioica* L.) produces silky cellulosic fibres, as well as bioactive molecules. To improve the knowledge on nettle and enhance its opportunities of exploitation, a draft transcriptome of the "clone 13" (a fibre clone) is here presented. The transcriptome of whole internodes sampled at the top and middle of the stem is then compared with the core and cortical tissues sampled at the bottom. Young internodes show an enrichment in genes involved in the biosynthesis of phytohormones (auxins and jasmonic acid) and secondary metabolites (flavonoids). The core of internodes collected at the bottom of the stem is enriched in genes partaking in different aspects of secondary cell wall formation (cellulose, hemicellulose, lignin biosynthesis), while the cortical tissues reveal the presence of a C starvation signal probably due to the UDP-glucose demand necessary for the thickening phase of bast fibres. Cell wall analysis indicates a difference in rhamnogalacturonan structure/composition of mature bast fibres, as evidenced by the higher levels of galactose measured, as well as the occurrence of more water-soluble pectins in elongating internodes. The targeted quantification of phenolics shows that the middle internode and the cortical tissues at the bottom have higher contents than top internodes. Ultrastructural analyses reveal the presence of a gelatinous layer in bast fibres with a lamellar structure. The data presented will be an important resource and reference for future molecular studies on a neglected fibre crop.

KEYWORDS
bast fibres, electron microscopy, immunohistochemistry, RNA-Seq cell wall composition, *Urtica dioica* L.

1 | INTRODUCTION

Harnessing plant biomass as energy feedstock and source of (macro) molecules for industrial applications is an undeniable need to foster a sustainable, low C bio-economy. Herbaceous crops are important renewable resources, because they produce biomass in a shorter time as compared to woody species.

Among herbaceous crops, plants producing bast fibres (belonging to the group of fibre crops) are very attractive, because they provide long and strong fibres containing high amounts of crystalline cellulose. These fibres are not only used in the textile sector, but are also appreciated by the biocomposite industry as eco-friendly alternatives to man-made fibres.

Flax, hemp, ramie and nettle produce bast fibres with gelatinous cell walls characterized by a high content of crystalline cellulose (>70%) and hypolignified (lignin content between 2%–7%) (Guerriero, Behr, Backes, et al., 2017; Guerriero, Sergeant, & Hausman, 2013). Several papers have been published on the molecular study of bast fibre formation in flax, ramie and hemp, however no study is yet available on stinging nettle (*Urtica dioica* L.), which is one of the most undervalued plants among the economically interesting ones.

Nettle is a perennial herbaceous plant growing in temperate regions and producing long bast fibres between 43–58 mm (Bacci, Baronti, Predieri, & di Virgilio, 2009) with high tensile strength. It has a long history as a fibre crop in Austria and Germany and was widely cultivated during the Second World War in Central Europe to manufacture the uniforms of the German army.

Urtica dioica grows well on over-fertilized soils, it is naturally resistant to pests and diseases and it is a robust weed relying on an underground system of roots and rhizomes. This fibre crop has a multitude of applications in the medicinal, textile and biocomposite sectors and is therefore a multi-purpose crop: its fibres are silkier in texture than flax, it can be used to treat skin conditions and has expectorant, hemostatic, anti-inflammatory and diuretic properties (Kregiel, Pawlikowska, & Antolak, 2018).

Similarly to hemp, the nettle stem is composed of a cortex containing bast fibres and a woody core. It has been shown that the stem of nettle displays a lignification gradient from the top to the bottom (necessary for mechanical strength at the stem base), accompanied by different stages of bast fibre development (from elongation at the top, to cell wall thickening at the bottom) (Backes et al., 2018). The differential cell wall composition of nettle stem tissues and the sequential developmental stages of bast fibres make this plant ideal to address bast fibre- and cell wall-related studies, as previously shown in textile hemp.

The availability of an annotated transcriptome is important for plant molecular studies and for addressing fundamental questions related to the function of specific genes.

We here provide for the first time a draft transcriptome of the nettle "clone 13" selected by Bredemann for fibre yield between 1927–1950 (Harwood & Edom, 2012). This clone is characterized by a higher bast fibre yield (16% as compared to wild nettle, which produces around 4%–5% bast fibres; Hartl & Vogl, 2002; Harwood & Edom, 2012).

The present study also provides the transcriptomic signature of nettle internodes sampled at different stem heights (top, middle and bottom which reflect progressive maturation stages of extraxylary fibres and vascular tissues) and gives a special emphasis to cell wall-related processes. The results are discussed in relation to the current knowledge concerning bast fibre development in other fibre crops, namely flax, hemp and ramie. The data are complemented by the chemical analysis of the cell walls extracted from the different internodes, the quantification of flavonoids and by the immunolocalization of specific polysaccharide components.

2 | METHODS

2.1 | Plant material, growth conditions and confocal microscopy

Urtica dioica was propagated via stem cuttings and grown in incubators following a cycle of 16 hr light 25°C/8 hr dark 20°C. After 5 weeks, stem internodes were collected along three regions of the stem localized at different heights (i.e., top, middle and bottom, as described in Guerriero, Behr, Legay, et al., 2017). Three biological replicates were used, each consisting of seven nettle plants selected among all incubators. The "TOP" segment is located at the top (below the apex). The "MID" (middle) is the segment possibly including the snap point and the "BOT" (bottom) segment corresponds to the second internode below the "MID". A segment of 2.5 cm was collected from the middle of each internode to minimise variations in gene expression, caused by the differences in developmental stages of the tissues (Guerriero, Behr, Legay, et al., 2017). The TOP and MID internodes were taken as a whole, following a sampling strategy previously published for flax (Gorshkov, Behr, Legay, et al., 2017). The BOT sample was peeled to separate the cortex from the core. The total sample numbers was therefore 12 (three biological replicates for the TOP, three for the MID, three for the BOT core and three for the BOT peels). In order to generate the de novo transcriptome, the reads obtained for the internodes of the three above-described stem regions were pooled with those obtained for other nettle tissues (leaves, roots, whole stem core tissues and peels, calli). The calli were sampled from in vitro-micropropagated nettle stems (according to Gatti, Di Virgilio, & Bacci, 2008). Young leaves were taken from the stem apex, while roots (fine roots) were quickly sampled, washed under tap water to remove soil particles, blotted dry and cut to smaller pieces with a sterile scalpel. All collected samples were frozen in liquid nitrogen and stored at −80°C until analysis. The libraries used to enrich the de novo transcriptome (i.e., those obtained using leaves, whole stems, roots and calli) were run as single replicates.

Sample preparation for confocal microscopy analysis with the different antibodies (PlantProbes) was carried out as previously described (Behr et al., 2016).

2.2 | Immunogold electron microscopy

The different internodes were sampled and immediately fixed for 2 hr at room temperature and overnight at 4°C in a mixture of 2% glutaraldehyde and 1.6% paraformaldehyde in 0.1 M phosphate buffer pH 6.9. Samples were washed with phosphate buffer twice for 10 min, then dehydrated in a graded series of ethanol. Samples were progressively embedded with LR-White resin from 1:1 ratio with ethanol to pure resin. After polymerization of resin for 2 days at 40°C, ultrafine sections were obtained with a diamond knife and the ultramicrotome LKB NOVA. For immuno-localization, sections of nettle internodes were collected on gold grids and blocked for 20 min with normal goat serum (NGS) diluted 1:30 in dilution buffer (0.05 M Tris-HCl pH 7.6, 0.9% NaCl and 0.2% BSA). Sections were incubated for 4 h at room temperature with primary antibodies LM10 for unsubstituted/low substituted xylans (PlantProbes, www.plantprobes.net) diluted 1:5 in the same buffer. Sections were washed for 20 min in the dilution buffer + 0.1% Tween20 and incubated for 45 min at room temperature with 10 nm gold particle-conjugated anti-rat secondary antibody diluted 1:20 in 0.02 M Tris-HCl pH 8.2. To visualize crystalline cellulose, the CBM3a protein was used at 5 µg/ml for 1.5 hr in conjunction with the mouse monoclonal anti-His antibody diluted 1:100 in dilution buffer + 0.1% Tween20 for 1.5 hr. Samples were washed and incubated with the anti-mouse antibody conjugated with 10 nm gold particles for 45 min at room temperature. All sections were visualized with the Philips MORGAGNI 268 80 kV transmission electron microscope, equipped with MEGAview II camera and elaborated with the Analysis software.

2.3 | Isolation and fractionation of cell wall material

Cell wall materials of all defined stem regions (TOP, MID, FBOT and CBOT), including four biological replicates of each region, were extracted as described previously (Pettolino, Walsh, Fincher, & Bacic, 2012) with some modifications. Briefly, about 50 mg of the ground lyophilized material were first extracted three times with 1.5 ml of 70% (v/v) ethanol at room temperature, one time with acetone and finally one time with methanol. The residues were dried using rotary evaporation and subsequently resuspended in 1.5 ml of acetate buffer (0.1 M, pH 5) in a thermomixer at 1,000 rpm and 80°C for 20 min. After cooling to 37°C, 10 U α-amylase (porcine pancreas, Sigma) and 8 U amyloglucosidase (*Aspergilus niger,* Sigma) were added to destarch the residues at 37°C overnight. Cell wall materials were then precipitated by four volumes of cold ethanol at −20°C for 3 hr, followed by washing with cold ethanol three times. Cell wall materials were air-dried and 15 mg were subjected to sequential extraction using water, 0.1% (w/v) EDTA (pH 7.5), 1 M KOH and 4 M KOH. The extractions were carried out three times with water and EDTA at 99°C for 2 hr each, respectively. Alkaline extractions supplemented with 0.01 mM NaBH$_4$ were performed one time at room temperature for 2 hr, after which the extracts were neutralized with glacial acetic acid. All extracts were dialyzed against deionized water and concentrated by rotary evaporation. The remaining residues after sequential extraction were rinsed three times with deionized water. All fractions and residues were freeze-dried and the yield was determined.

2.4 | Chemical composition analysis of cell wall fractions

About 5 mg of each fraction and the remaining cell wall residue were incubated with 500 µl trifluoroacetic acid (2 M) at 99°C for 2.5 hr, respectively. The hydrolysate was diluted 1:2 and 1:100 with water for further analyses. The monosaccharide composition was determined for each sample in duplicate using a Dionex™ ICS-5000$^+$ Capillary HPIC™ System with a pulsed electrochemical detector (Thermo Scientific™ Dionex™). The separation of each monosaccharide was performed with a CarboPac PA20 analytic column (3 × 150 mm, Thermo Scientific™ Dionex™) and a CarboPac SA10 analytic column (2 × 250 mm, Thermo Scientific™ Dionex™). The eluents were 300 mM NaOH, 1 mM NaOH and deionized water. For the PA20 column, the separation of monosaccharides was carried out using 4% 1 mM NaOH at a flow rate of 0.5 ml/min at 30°C. For SA10 column, 100% 1 mM NaOH was used to separate the monosaccharide at a constant flow rate of 0.38 ml/min at 45°C. The retention time (RT) obtained with a single injection of each sugar was used to characterize the monosaccharides of the cell wall. Data acquisition and analysis were carried out using Chromeleon™ Chromatography Data System (CDS) Software (Thermo Scientific™). The sugars detected were fucose (Fuc), rhamnose (Rha), arabinose (Ara), galactose (Gal), glucose (Glc), xylose (Xyl) and mannose (Man). The amount of each monosaccharide was quantified against a calibration curve, which was obtained by varying standard concentrations (1, 2.5, 5, 7.5, 10, 25, 50, 75, 100 µmol/L). Significant differences in the yield of fractions and the amount of each monosaccharide among samples were determined at $p < 0.05$ by an ANOVA one-way analysis and Tukey's post-hoc test using SPSS 13.0 (SPSS Inc.).

2.5 | Extraction of polyphenols and HPLC analysis

The nettle internodes were sampled as previously described and the powder obtained was then lyophilized for 2 days. Ten mg of dry powdered material was dissolved in 2 ml of acidified methanol containing 1% (v/v) HCl. The standard procedure used for acid hydrolysis of the flavonoids was previously described (Tokuşoglu, Ünal, & Yildirim, 2003). The solution was incubated at 90°C for 2 hr and continuously stirred. The sample was sonicated and cooled at room temperature for 3 min to remove free oxygen generated by the reaction. The final extract was filtered through a 0.45 µm membrane filter. The solution was then concentrated for 2 hr in a vacuum concentrator centrifugal evaporator (Model RC10-10; Jouan SA) and then resuspended in a volume of 200 µl before the HPLC injection. The HPLC method was adapted from a method reported previously (Berni, Romi, et al., 2018). The analysis was carried out with an RP-C18 column (SUPELCO; Kromasil 100A-5u-C18 4.6 mm × 250 mm), at a flow rate 1 ml/min and the absorbance set at 280 nm, in a run time

of 21 min. The mobile phase consisted of two solutions, (A) H2O and (B) acetonitrile with 0.02% trifluoroacetic acid and the following gradient: 0–5 min A (20%)–B (80%); 5–8 min A (60%)–B (40%); 8–12 min A (50%)–B (50%); 12–17 min A (60%)–B (40%); 17–21 min A (80%)–B (20%). Quantification was performed using an external standard calibration curve consisting of six points at the increasing concentrations of 0.5, 2, 5, 12, 25, and 50 µg/ml for each standard components used (e.g., (+)-catechins hydrate, rutin hydrate, vanillic acid, kaempferol, quercetin hydrate, isorhamnetin hydrate; Sigma Chemical). A one-way ANOVA with Tukey's post-hoc test was carried out on log10 transformed values.

2.6 | RNA extraction

Samples were reduced to a fine powder using a mortar, a pestle and liquid nitrogen. Total RNA was extracted using the RNeasy Plant Mini Kit (Qiagen) following the manufacturer's instructions (with the on-column DNase digestion), as described in Guerriero, Mangeot-Peter, et al. (2017) and Mangeot-Peter, Legay, Hausman, Esposito, and Guerriero (2016). RNA quantity and quality were assessed with a NanoDrop ND-1000 spectrophotometer (Thermo Scientific) and a 2100 Bioanalyzer (Agilent). All the RNAs displayed a RIN above 8.

2.7 | Preparation of the libraries, processing of the reads, mapping, transcriptome assembly and RNA-Seq analysis

Libraries were prepared, quantified and their average size determined as previously described (Guerriero, Behr, Legay, et al., 2017). The libraries were pooled (the 12 samples corresponding to the 3 stem regions) or run alone (the leaves, roots, calli, whole stem tissues) after normalising them to 20 pM and sequenced on an Illumina MiSeq. The pooled 12 libraries were sequenced in a total of 6 consecutive runs (5 MiSeq reagent kit V3, 150 cycles and 1 run of 300 cycles); the libraries obtained for the leaves, roots, calli, whole stem core and peels were each run using the MiSeq kit 300 cycles. Raw sequences have been deposited at the Sequence Read Archive (SRA) with the accession number PRJNA518071. The raw sequences were downloaded from BaseSpace and uploaded in CLC Genomics Workbench v. 9.0.1. Sequences were filtered as follows: sequences > 35 bps, the sequence quality score was left as default value (0.05), the maximum number of ambiguities was set to 0. Adaptor trimming was performed using the Illumina adaptor sequences, then for the libraries run using 150 cycles a hard trim of 15 bps at the 5′ end and 3 bps at the 3′ end was additionally carried out, resulting in a final sequence average length of 57 bps. For the libraries sequenced using the kit with 300 cycles, 15 bps were removed at the 5′ and 80 at the 3′ (final average length 205 bps). Additionally, the sequences with a length <35 bps (for the libraries run using the kit with 150 cycles) and <65 bps (for those sequenced with 600 cycles) were removed.

The parameters used for the de novo transcriptome assembly were: wording size was set to 20, the bubble size to 50 and minimum contig length of 300. The reads were mapped back to the assembly with a mismatch, insertion and deletion cost of 3 (stringent criteria), and a length and similarity fraction of 0.95. The assembly was then annotated using Blast2GO PRO version 3.0 against the *Arabidopsis thaliana* non-redundant database. For each of the 12 libraries, the mapping was performed with a maximum hit per read of 3, a similarity and length fraction of 0.95, a mismatch, insertion and deletion cost of 3. The expression values were then calculated using the RPKM method (Mortazavi, Williams, McCue, Schaeffer, & Wold, 2008).

The expression values were subjected to an ANOVA statistical test with four groups (TOP, MID, BOT CORE and BOT FIBRES), each composed of three biological replicates and, subsequently, to a false discovery rate (FDR) correction. Only those genes showing a corrected p-value < 0.05 were retained for downstream analysis. The data were further filtered by removing the genes showing a maximum value of the means < 1 RPKM and a maximum FC>|4|. A total of 1,663 contigs were obtained (Data S1 File).

2.8 | cDNA synthesis and RT-qPCR

One microgram of RNA was retrotranscribed using the ProtoScript II RTase (NEB), following the manufacturer's instructions. Gene primers were designed with "Primer3Plus" (http://www.bioinformatics.nl/cgi-bin/primer3plus/primer3plus.cgi) and checked using the software OligoAnalyzer 3.1 tool from Integrated DNA technologies (http://eu.idtdna.com/calc/analyzer). Efficiencies were calculated by RT-qPCR with a calibration curve consisting of six serial dilutions of cDNA (10, 2, 0.4, 0.08, 0.016, 0.0032 ng/µl). The list of primers is given in Data S1.

The RNA extracted using the above-mentioned protocol was retrotranscribed into cDNA using the ProtoScript II RTase (NEB) and random primers, according to the manufacturer's instructions and as described in. The cDNA was diluted to 2 ng/µl and 2 µl were used for the RT-qPCR analysis in 384-wells microplates (final volume: 10 µl). An automated liquid handling robot (epMotion 5073) was used to prepare the microplates. The expression of each target gene was normalized using 2 genes (*EF2* and *eTIF4E*) chosen among the recently reported nettle reference genes (Backes et al., 2018). A melt curve analysis was performed to check the specificity of the amplicons. The relative expression of the genes was calculated in qBase^PLUS (Hellemans, Mortier, De Paepe, Speleman, & Vandesompele, 2007) with the above-mentioned 2 reference genes.

2.9 | Bioinformatics

Putative TFs in the de novo assembly were annotated with PlantTFcat (http://plantgrn.noble.org/PlantTFcat/) and iTAK (Zheng et al., 2016), which gave a total of TFs, respectively (Data S1 File).

The Gene Ontology term Enrichment analysis (GOE) was performed using ShinyGO (available at: http://ge-lab.org:3838/go/) and Cytoscape (v3.4.0) with the ClueGO v2.3.2 plugin (Bindea et al., 2009) (p-value < 0.05, Benjamini-Hochberg enrichment, gene ontology from level 3 to 8, kappa score set at 0.4).

3 | RESULTS AND DISCUSSION

3.1 | Yield of cell wall fractions

Cell wall materials of the different regions of nettle stem, namely TOP, MID (middle), CBOT (core tissue at the bottom) and FBOT (cortical tissues at the bottom), were isolated and subjected to a series of chemical extractions. The sequential extraction used aimed at extracting pectin polysaccharides with hot water and EDTA and then hemicelluloses with 1 M and 4 M KOH. To compare the yield of each fraction among different samples and eliminate the effect of the possible incomplete dialysis, the yield of each fraction was expressed as a percentage of the total weight of four fractions (Figure 1a).

Hot water extracted a significantly higher amount of pectin polysaccharides from MID (27.2% ± 2.2%) as compared to CBOT (19.1% ± 4.9%) and FBOT (20.5% ± 2.0%; $p < 0.05$). In contrast, the yield of the EDTA fraction was significantly higher in FBOT than in TOP, MID and CBOT ($p < 0.01$) and, most notably, 44% higher relative to MID (Figure 1a). It is known that hot water can only partially solubilize some of the pectic substances of the primary cell walls and middle lamella, whereas EDTA is able to extract the pectic substances that are complexed with Ca^{2+}, namely Ca^{2+}-pectate gels (Selvendran & O'Neill, 1987). Taken together, these results show that more water-soluble pectins were present in the MID, where bast fibres are elongating, while more Ca^{2+}-pectate gels were present in the FBOT, where the elongation of the fibre cells is completed.
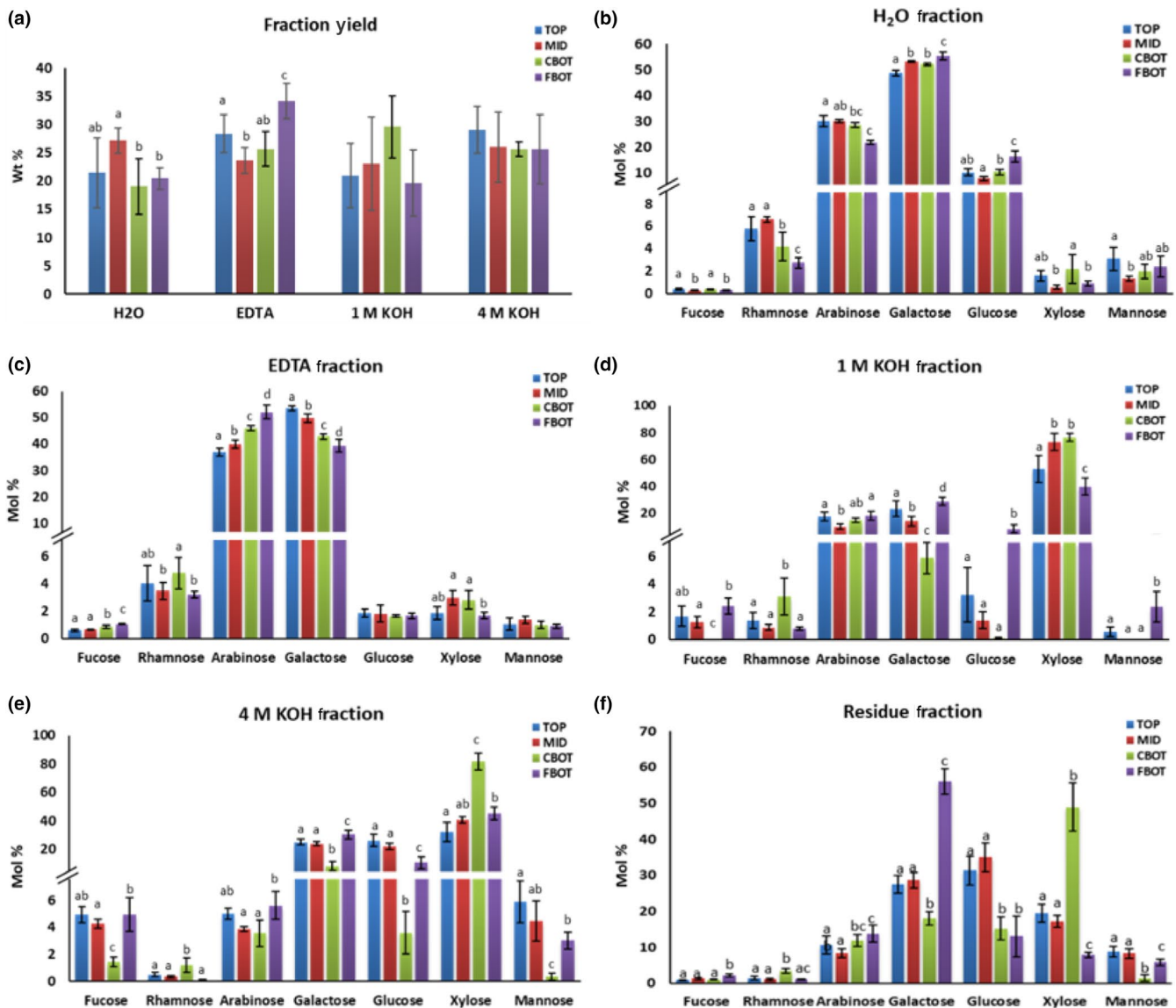

FIGURE 1 Yield of cell wall fractions from different regions of the nettle stem (a) and monosaccharide composition of the cell wall fraction obtained by hot water (b), EDTA (c), 1 M KOH (d), 4 M KOH (e) and the remaining residue (f). TOP, MID, CBOT and FBOT represent the top, middle, bottom core and bottom fibre of the nettle stem, respectively. Values are expressed as the mean ± *SD* from four biological replicates and two technical replicates. Significant differences were analysed using a one-way ANOVA with Tukey's post-hoc test. Letters (a–d) indicate statistically significant differences between groups at $p < 0.05$

Our finding re-enforces the view that the solubility of pectin in the middle lamella and fibre cell wall decreases with the fibre maturity along the stem. On the one hand, more water-soluble pectins are possibly required in the middle lamella and the tip of elongating fibres to facilitate the intrusive tip growth of bast fibres. This is in agreement with previous studies, which demonstrated that more soluble pectins confer a positive effect on the fibre length of hybrid aspen plants (Pelloux, Rustérucci, & Mellerowicz, 2007; Siedlecka et al., 2008) and the expansion of the pollen tube (Li, Chen, Linskens, & Cresti, 1994). However, more Ca^{2+}-pectate gels are present in the bottom region of the nettle stem and this could be explained if we consider that Ca^{2+}-pectate gels can strengthen cellular adhesion and rigidify the cell walls (Snegireva et al., 2010).

In addition, there was no significant difference in the yield of both KOH fractions among samples, although the 1 M KOH fraction of CBOT showed a considerable increase compared to that of the other samples, possibly due to the high xylan content (Figure 1a).

3.2 | Chemical composition of the cell wall

To further investigate the chemical composition of the cell wall, the monosaccharide composition was analysed for each fraction and the remaining residue after TFA hydrolysis. As shown in Figure 1b, the hot water fraction of all samples contained predominantly Rha (rhamnose), Gal (galactose) and Ara (arabinose), indicating the presence of rhamnogalacturonan (RG) polymers. FBOT shows significantly lower amounts of Rha and Ara than TOP and MID, whereas it displays significantly higher amounts of Gal than TOP, MID and CBOT ($p < 0.05$, Figure 1b). These results suggest a distinct composition or structure of RG in the FBOT as compared to the other regions of the stem. The presence of small amounts of Xyl (xylose), Fuc (fucose) and Man (mannose) in all samples indicates the occurrence of these sugars on the side chains of RG which was also previously observed in the water-soluble fraction of hemp fibres (Crônier, Monties, & Chabbert, 2005). In this same study, the authors suggested that water-soluble glucomannans were largely distributed in the middle lamella based on the presence of high amount of Glc (glucose) and Man in the water extract and the microscopic observations of fibres after water extraction. Additionally, water-soluble glucomannans were also found in flax bast fibres, but to a lesser extent than hemp (Goubet et al., 1995; Jacobs, Palm, Zacchi, & Dahlman, 2003). In the present study, the average amount of Man content in the FBOT is 2.4%, which is remarkably lower than that observed in mature hemp fibres (basal regions, 12.3% at "full" flowering stage and 22.5% at grain maturity stage) (Crônier et al., 2005). In order to confirm the presence of the water-soluble glucomannan in nettle, further investigations are needed; however, the results obtained suggest the presence of differences in the composition of hemp and nettle bast fibres.

The EDTA fraction of all samples shows a similar sugar composition to the hot water fraction, in which the predominant sugars are Ara and Gal (Figure 1c). Although Ara and Gal are the primary side chain sugars of RG, we cannot rule out the possibility that they

may partially derive from arabinogalactan proteins (AGPs). This is because AGPs were demonstrated to be ubiquitous cell wall components and to play an important role in the regulation of fibre development in cotton (Huang et al., 2013), flax (Roach & Deyholos, 2007, 2008), hemp (Guerriero, Mangeot-Peter, et al., 2017) and poplar (Wang et al., 2015). Moreover, it was also shown that AGPs are present in the hot water and EDTA extract of the cell wall of *Craterostigma wilmsii* (Vicré, Lerouxel, Farrant, Lerouge, & Driouich, 2004).

As shown in Figure 1d, Xyl is the predominant monosaccharide in the 1 M KOH fraction of all samples, demonstrating its hemicellulosic nature. Generally, large differences in the amount of monosaccharides are evident between CBOT and FBOT, while each monosaccharide in both TOP and MID shows values in-between those of CBOT and FBOT (Figure 1d). This may be because the TOP and MID segments were not peeled to separate the core and cortex, thereby leading to a mixed characteristic.

Interestingly, CBOT shows a 2-fold increase in Xyl content with respect to FBOT, while the amount of Fuc, Glc and Gal was significantly lower in CBOT as compared to FBOT ($p < 0.001$, Figure 1d). We therefore reason that large amounts of Xyl in the CBOT, on average 76.4% of the total sugars, most likely derive from xylan rather than xyloglucan. In contrast, xyloglucan could be the major hemicellulosic polysaccharides in the FBOT due to the high amount of Fuc, Glc, Gal and Xyl (Figure 1d). The presence of xylan in CBOT is further supported by the immunohistochemical analyses with the LM10 antibody. No LM10 labelling was observed in the nettle bast fibres (FBOT) (Figure S1). Interestingly, the immunoTEM analyses reveal the presence of a G-layer that is "flaking off" (Figure S1E): if the lack of an LM10 signal is taken into account, one could associate this phenotype to the absence of xylan in the S1-layer enveloping the gelatinous cell walls of bast fibres. It remains to be unequivocally demonstrated whether xylans are really absent from nettle bast fibres. LM10 was recently shown to be specific for the non-reducing end of xylans (Ruprecht et al., 2017). We cannot exclude the possibility that the lack of an LM10 signal is due to the presence of highly substituted xylans in the nettle bast fibres, or to the masking of the non-reducing end, or to both.

For the 4 M KOH fraction, the amount of each monosaccharide among samples displays a pattern that was similar to 1 M KOH fraction (Figure 1e). However, the amount of Fuc, Gal and Glc in CBOT is largely higher compared to that in the 1 M KOH fraction (Figure 1e), implying the presence of xyloglucan in the 4 M KOH fraction of CBOT.

Although the remaining cell wall residue after sequential extraction was expected to contain mainly cellulose, the analysis of its monosaccharide composition shows the presence of non-cellulosic polysaccharides (Figure 1f). These non-cellulosic polysaccharides could be tightly bound to cellulose, therefore they cannot be easily extracted by the sequential chemical treatment. Strikingly, the results show a remarkable high amount of Xyl in CBOT and of Gal in FBOT, representing 48.9% and 56.1% of total sugars, respectively (Figure 1f). The former result could be due to the high xylan content

in the CBOT, as suggested by the data of both KOH fractions. The latter finding suggests that galactan-containing polymers could play a prominent role in secondary cell wall (SCW) formation of nettle fibres, as previously suggested for flax (Gorshkova et al., 2004; Goubet et al., 1995) and hemp (Crônier et al., 2005).

3.3 | Draft transcriptome of stinging nettle and RNA-Seq analysis

The first step to carry out a high-throughput gene expression analysis in the stem internodes was to obtain a first draft transcriptome. The de novo transcriptome of the nettle fibre clone, known as "clone 13", was obtained by merging the reads generated from the sequencing of cDNA libraries of different tissues/organs. More specifically these are roots, leaves, undifferentiated calli forming at the tip of cuttings used for in vitro propagation (Gatti et al., 2008), as well as cortical tissues obtained from internodes along the whole height of the plant. We reasoned that the inclusion of other tissue types would increase the accuracy of the de novo assembly, by providing reads for genes expressed at low levels in stem tissues. These reads were merged with those obtained for the analysis of internodes at different developmental stages (TOP, MID and BOT). A total of 36,320 contigs with an N50 of 1,150 bp were obtained, which is in the same order of magnitude as the values reported previously for the other *Urticaceae* member *Boehmeria nivea* (Al-Ani & Deyholos, 2018) and for textile hemp (Guerriero, Behr, Legay, et al., 2017). Mapping of the reads back to the assembly gave an average 80%, indicative of a good quality (Carruthers et al., 2018; Haas et al., 2013). The annotation of transcription factors (TFs) resulted in the identification of 2,435 contigs coding for members belonging to different families (Data S1). In textile hemp Santhica 27, we previously annotated approximately the same number of contigs (2,484) as TFs (Guerriero, Behr, Legay, et al., 2017). A more detailed investigation of specific families known to play a role in cell wall biosynthesis (Nakano, Yamaguchi, Endo, Rejab, & Ohtani, 2015) and secondary growth (Yordanov, Regan, & Busov, 2010) identified 50 members of the MYB family, 49 of the NAC, 17 of the LOB (LATERAL ORGAN BOUNDARIES) domain and 4 PLATZ TFs (Data S1).

The Principal Component Analysis (PCA) of the RNA-Seq data shows a good separation of the TOP/MID and BOT samples, as well as the CBOT and FBOT (Figure 2). The TOP and MID samples cluster instead together; the biological replicates of each stem region or tissues sampled also group tightly together.

The first 2 components, PC1 and PC2, explain 93% of the total variance. More specifically, PC1 represent 61% of the total variance, while PC2 32%. PCA pathways analysis carried out using iDEP (Ge, Son, & Yao, 2018) shows that the discrimination along the first component is on the basis of pathways related to cell wall-related processes, while the separation along the second component involves processes related to monocarboxylic acid metabolism and organ development (Table 1).

The hierarchical clustering of RNA-Seq data performed with Cluster 3.0 (Eisen, Spellman, Brown, & Botstein, 1998) using a
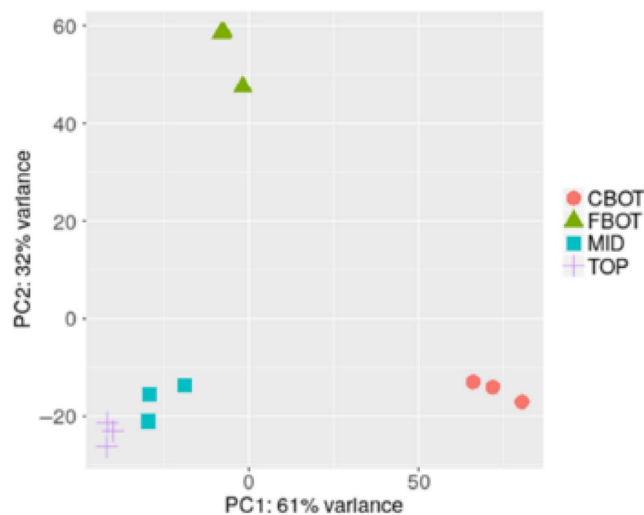

FIGURE 2 Principal Component Analysis (PCA) of the different stem regions sampled

Pearson correlation > 0.5 shows the presence of eight gene expression clusters, hereafter referred to as C1-C8 (Figure 3 and Data S1). The first group, C1, is composed of 121 contigs, while the second, C2, of 302 contigs. Their expression profiles show a peak in the bottom tissues containing the bast fibres (FBOT). Clusters C3 (123 contigs) and C4 (509 contigs) show highest expression in the core tissues at the bottom (CBOT), while clusters C5 (286 contigs) and C6 (260 contigs) show the opposite trend, i.e., lowest expression at the CBOT. The last clusters C7 and C8 are represented by a smaller number of contigs, 48 and 12, respectively; C7 shows lowest expression at the FBOT, while C8 has the highest expression at the middle.

In order to shed light on the major gene ontologies associated with each stem region and tissue type, a gene ontology enrichment (GOE) analysis was performed using Cytoscape (v3.5.1) with the ClueGO v2.5.0 plugin (Benjamini-Hochberg-corrected p-values, biological process enrichment, GO from level 3 to 8, kappa score set at 0.4). Six of the eight gene expression clusters (C1–C6) showed a statistically significant enrichment of GO terms ($p < 0.05$). We will hereafter analyse the major processes associated with each nettle

TABLE 1 Pathway analysis on the PCA

Component	Pathways	e-Value
PC1	Plant-type cell wall biogenesis	3e−03
	Cell wall biogenesis	9e−04
	Cellular component biogenesis	2e−03
	Cellular carbohydrate metabolic process	7e−03
	Cell wall organization or biogenesis	2e−01
PC2	Monocarboxylic acid metabolic process	7e−03
	Phyllome development	2e−01
	Multi-organism process	6e−02
	Plant organ development	2e−02

Note: The e-values corresponding to each pathway are provided.
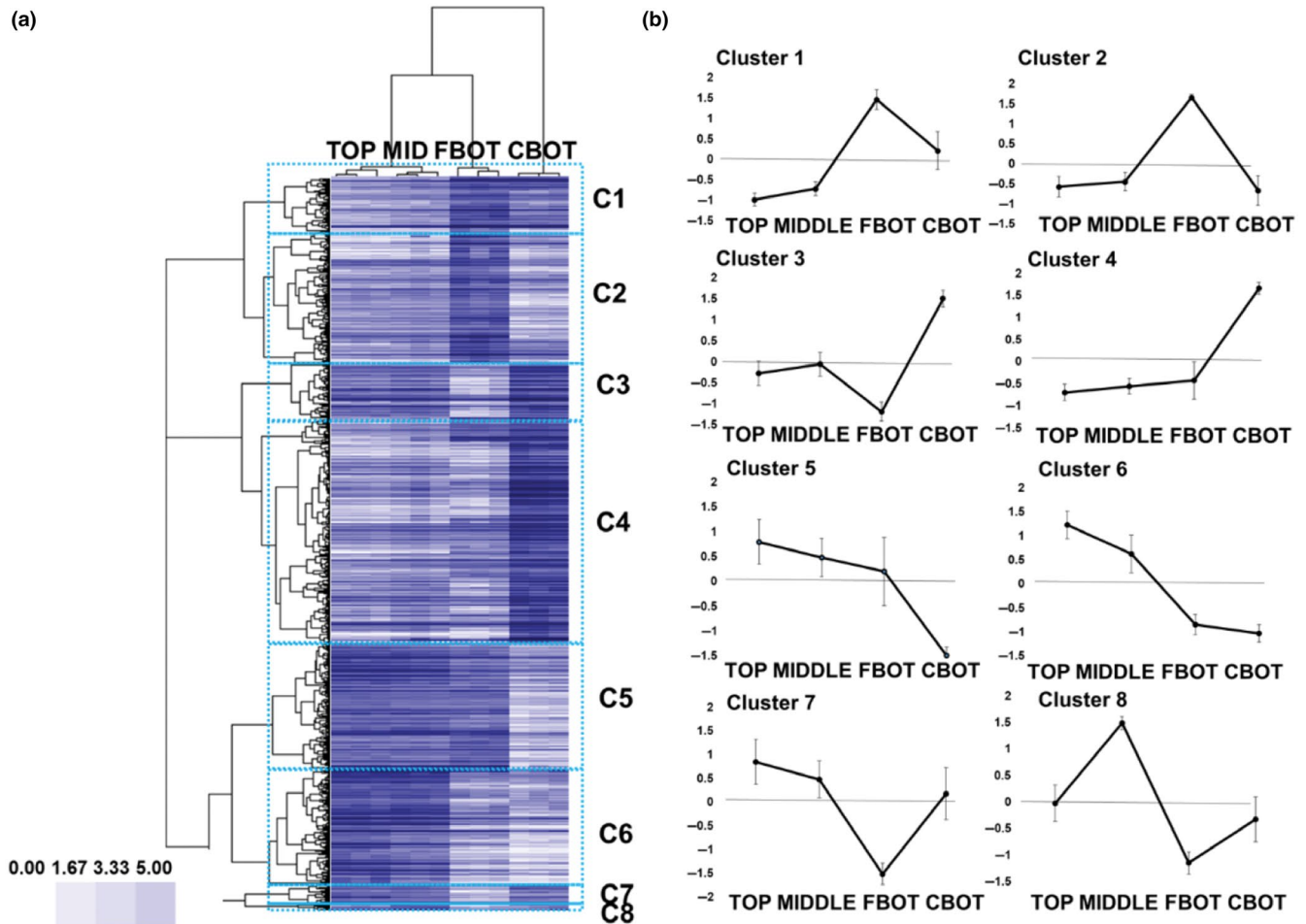
(a)

(b)

FIGURE 3 (a) Heat map hierarchical clustering of the RNA-Seq data. C1–C8 clusters obtained using a Pearson correlation > 0.5. The scale bar indicates the expression intensities. (b) Profiles of the eight clusters of genes obtained using a Pearson coefficient > 0.5. The profiles are relative to the log2RPKM rescaled values ± standard deviation (the rescaled values were obtained by subtracting the mean contig expression value of the four stem tissues and dividing by the standard deviation)

internode/stem tissue at the different heights. We will follow the cluster numberings (from C1 to C6) for the presentation and discussion of the results.

3.4 | GOE analysis of the cortical tissues at the bottom

For C1, the GOE analysis revealed enrichment in genes partaking in the response to sugars (hexoses) and in the aspartate family amino acid metabolic process (Data S1). These are *asparagine synthetase 1* (*ASN1* corresponding to three different contigs, each showing > 4.5 fold increase when comparing FBOT vs. TOP and >3 fold for FBOT vs. MID), *DORMANCY-ASSOCIATED PROTEIN-LIKE 1* (*DYL1*, FBOT vs. TOP > 8.5, FBOT vs. MID > 6) and *extra-large guanine nucleotide-binding protein 1* (*XLG1*, FBOT vs. TOP > 7, FBOT vs. MID > 3).

ASN1 is an important enzyme in plant primary metabolism, as it regulates N levels (Hwang, An, & Hwang, 2011). The model plant thale cress has three genes encoding ASN; more specifically, only *ASN1* is responsive to the endogenous sucrose levels (Lam, Hsieh, &

Coruzzi, 1998). Sucrose inhibits the expression of *ASN1* via a cascade relying on the S1 class of bZIP TFs (Curtis, Bo, Tucker, & Halford, 2018; Hummel, Rahmani, Smeekens, & Hanson, 2009). Notably, in our dataset, the *bZIP9* gene showed an increase >4- and >3-fold when comparing FBOT vs. TOP and MID, respectively (Data S1). According to our results, the nettle ortholog of *AtASN1* was upregulated in the cortical tissues at the BOT, suggesting the presence of a C (sugar) depletion signal in these tissues.

The expression pattern of other genes in this cluster corroborates the hypothesis of a C starvation syndrome in the cortical tissues sampled at the bottom. *DYL1/DRM1* is a sugar starvation marker (Gonzali et al., 2006; Tarancón, González-Grandío, Oliveros, Nicolas, & Cubas, 2017) that is overexpressed when the endogenous sugar levels are low. The higher expression of this gene in the nettle cortical tissues at the bottom indicates the presence of a C-starvation status, likely induced, as described in more detail below, by the UDP-glucose demand necessary for the thickening phase of bast fibres.

XLG proteins are composed of three members in thale cress and are ubiquitously expressed, with a preference in vascular tissues

(Ding, Pandey, & Assmann, 2008): *Arabidopsis xlg* triple mutants displayed increased length of the primary root when grown in the dark and also showed an altered sensitivity to sugars. It was proposed that the *xlg* phenotype may be due to an altered glucose sensing, although a sucrose-specific mechanism was also invoked (Ding et al., 2008). In the dataset here presented, the upregulation of *XLG1* in the peels of the bottom internode (fold-increase FBOT vs. MID > 3 and FBOT vs. TOP > 7) is likely related to a sucrose-sensing mechanism, as supported by the sucrose metabolism/transport-related transcripts induced in the same tissues (see below). It is interesting to mention here that the cotton *XLG1* gene was upregulated at 6 days post anthesis in the Ligon lintless 1 (*Li1*) mutant, which is characterized by short lint fibres and thickened SCW as compared to the wild-type isogenic line TM-1 (Liu, Sun, Yao, & Yuan, 2012). In the *Li1* mutant, notably, the starch and sucrose metabolisms were dysregulated (Liu et al., 2012).

The second cluster, C2, characterized by genes peaking in expression at FBOT, is dominated by ontologies related to polysaccharide localization and oligosaccharide biosynthesis, response to pathogens and salicylic acid (SA) stimulus, as well as wax metabolic process. This last process is likely due to the "contamination" caused by the epidermal cells present in the cortical peels and, therefore, it will not be discussed here, since the focus of the study is on bast fibre developmental aspects. The genes belonging to the response to SA stimulus are *AT4G03470*, *SAG29*, *WRKY70* (Data S1). These genes are likely related to senescence, since SA was shown to regulate leaf senescence (Morris et al., 2000) and *SAG29* (a.k.a *SWEET15*, a member of the *sugars will eventually be exported* transporters) is known to be expressed in senescing tissues (Seo, Park, Kang, Kim, & Park, 2011). *SAG29* showed among the highest levels of expression in the cortical tissues sampled at the bottom (FBOT vs. TOP/MID > 40): this sucrose transporter mediates sucrose unloading from the outer integument to the apoplasm in seeds (Chen et al., 2015) and can be involved in the transfer of sucrose to the thickening bast fibres. *AT4G03470* codes for an ankyrin-containing protein responding to SA stimulus; *WRKY70* is a regulator of the SA and jasmonic acid (JA) responses and acts by repressing the latter (Li, Brader, Kariola, & Palva, 2006). These genes hint at the existence of a SA response stimulus in the cortical tissues, which may regulate sucrose transfer from the phloem to the thickening bast fibres in the cortical tissues at the stem bottom. In this respect it should be noted that SA was previously shown to promote sucrose unloading in the root tips, at concentrations $<10^{-4}$ M (Burmistrova, Krasavina, & Akanov, 2009). Further studies are needed to confirm this hypothesis, as for example the analysis of SA and sucrose concentrations in the tissues sampled at different stem heights.

The genes in the oomycete response group further confirm the presence of a SA-responsive mechanism, since *SARD1* is essential for SA biosynthesis (Zhang et al., 2010) and *AT5G20230* (encoding a blue copper binding BCB protein) may be related to senescence, since it was shown that a *BCB* was upregulated during ozone-induced senescence of *Arabidopsis* rosettes (Miller, Arteca, & Pell, 1999). It should be noted that the presence of an oomycete response group does

not here imply biotic stress, as the plants were grown in a controlled environment devoid of any fungal/pseudofungal contamination. We here describe the genes in this group to strengthen the above link with the SA biosynthetic pathway.

In the process related to polysaccharide/callose localization there are the sucrose synthases *SUS5* and *SUS6*, together with *NSL1*, a gene encoding a membrane-attack complex/perforin (MACPF) containing protein. While the role of the sucrose synthases is clear, i.e., they produce UDP-glucose required for cellulose biosynthesis during the thickening phase of the bast fibres, the role of *NSL1* is more difficult to infer. In the literature, this protein represses the microbe-associated molecular patterns (MAMP)-related cell death (Fukunaga et al., 2017) and may be linked to senescence-related processes in older internodes of nettle stems.

A trehalose-6-phosphate phosphatase (*TPPI*) gene showed strong upregulation in the peels sampled at the bottom (FBOT vs. TOP/MID > 7). TPPs play an important role in developmental processes in relation to nutritional homeostasis and C balance (Vandesteene et al., 2012); hence, in nettle cortical tissues, TPPI may be involved in regulating the endogenous levels of trehalose-6-phosphate and, consequently, of the UDP-glucose pool required for the thickening of bast fibres.

The GOE results showed the presence of a process related to the remobilization of sucrose to bast fibres in an active stage of SCW biosynthesis. Bast fibres therefore act as sink tissues requiring photosynthates (in the form of sucrose) to sustain cellulose biosynthesis.

3.5 | GOE analysis of the bottom core tissues

The clusters C3 and C4 are characterized by those genes showing higher expression in the core tissues at the bottom. In C3, the GOE analysis reveals ontologies related to aromatic amino acid family metabolic process, amino acid export and vascular tissue development (Data S1). The upregulation of genes involved in aromatic amino acid biosynthesis indicates the supply of intermediates shunted to the phenylpropanoid pathway, a key secondary metabolic hub responsible for the synthesis of the lignin building blocks. Among such genes, it is here noteworthy to mention *EMB1144* (encoding chorismate synthase) and *EPSPS* (5-enolpyruvylshikimate-3-phosphate synthase; *At2g45300*) (CBOT vs. FBOT > 4.5 and >4.3, respectively; Data S1). The products of these genes are involved in chorismate formation, a central metabolite in the synthesis of aromatic amino acid, as well as secondary metabolites (Tzin & Galili, 2010).

In the phloem/xylem histogenesis ontogeny, the gene *ACL5* (*ACAULIS5*; *At5g19530*) is present, (corresponding to 2 contigs, contig 27116 with FC CBOT vs. FBOT > 26 and contig 17188 with FC > 11; Data S1): this gene codes for a thermospermine synthase (Knott, Römer, & Sumper, 2007) and was shown to be involved in stem elongation in thale cress (Hanzawa et al., 2000; Kakehi, Kuwashiro, Niitsu, & Takahashi, 2008). Mutants of this gene show premature cell death with xylem defects caused by the absence of fibres and of secondary cell walls in the vessels (Hanzawa et al., 2000; Moschou & Roubelakis-Angelakis, 2014; Muñiz et al., 2008).

The gene *HB-8* is also highly expressed in the CBOT (FC CBOT vs. FBOT = 4; Data S1) and it was shown to be regulated by auxin and to promote thermospermine biosynthesis in thale cress by binding to the BS-III *cis*-regulatory element in the promoter of *ACL5* (Baima et al., 2014). The expression of *HB-8* (and other *HD-ZIP III* genes, like those involved in auxin signalling) is regulated by ACL5 via a negative feedback loop. In nettle core tissues, there appears to exist a thermospermine/auxin-based mechanism controlling xylem formation. It will therefore be interesting to measure this metabolite in the different internodes of the nettle stem and also to measure the expression of PA (polyamine) oxidases (PAOs) to understand the dynamics of synthesis and catabolism.

In C4, the significantly enriched ontologies are mainly related to SCW biogenesis consisting of cellulose, xylan, lignin and pectin biosynthetic processes. This result is most likely to be associated with the developing xylem tissue in the CBOT, in which the deposition of thick SCW occurs during the maturation of xylem cells and contributes to the mechanical strength of nettle stem. In the "cellulose biosynthetic process" ontogeny, three genes encoding cellulose synthase (*CesA*) are present, namely *CesA4/IRX5* (cellulose synthase 4/irregular xylem 5; contig 15236, contig 9977 and contig 9978; Data S1), *CesA7/IRX3* (contig 22306) and *CesA8/IRX1* (contig 27738). The products of these *CesA*s were reported to form a functional trimer that is essential for cellulose synthesis in the SCW of developing xylem vessels (Hill, Hammudi, & Tien, 2014; Taylor, Howells, Huttly, Vickers, & Turner, 2003; Taylor, Laurie, & Turner, 2000; Taylor, Scheible, Cutler, Somerville, & Turner, 1999). In this study, the remarkable up-regulation of these genes in the core of the bottom stem strongly indicates an indispensable role of this protein trimer in the developing xylem of nettle, which is analogous to those reported for tree species, such as *Populus* (Joshi, 2003; Samuga & Joshi, 2002; Wu, Joshi, & Chiang, 2000) and loblolly pine (Nairn & Haselkorn, 2005). Moreover, the occurrence of crystalline cellulose in xylem tissue of bottom stem segments was confirmed by immunoTEM analyses carried out with the CBM3a recombinant protein which in our previous study labelled nettle bast fibres (Backes et al., 2018; Figure S2).

Genes involved in the "xylan biosythetic process" are highly expressed in the CBOT, indicating that xylan is the chief hemicellulosic polymers in the CBOT. This result is in agreement with our observation obtained from chemical analyses of cell wall components (Figure 1d,e) and immunohistochemical analyses of stem cross-sections (Figure S1).

In this ontogeny, we identified several genes that are associated with the glucuronoxylan biosynthesis, i.e. *IRX9* (contig 33467, Data S1), *IRX14-L* (IRX14-Like, contig 12654) and *IRX10-L/GUT1* (glucuronosyl tranferase 1), as well as *PGSIP1/GUX1* (plant glycogenin-like starch initiation protein 3/glucuronic acid substitution of xylan 1, contig 5780). IRX9 and IRX14-L are members of GT43 (glycosyltransferase family 43), while IRX10-L/GUT1 belongs to GT47; notably, they are all responsible for the elongation of the xylan backbone (Peña et al., 2007; Wu et al., 2010). PGSIP1/GUX1 is a member of

GT8 involved in adding glucuronic acid residues onto xylan (Lee, Teng, Zhong and Ye, 2012).

Glucuronoxylan methyltransferase (GXM) was reported to be responsible for catalysing 4-*O*-methylation of glucuronic acid side chains on xylan (Lee, Teng, Zhong, Yuan, et al., 2012). In CBOT, our data showed that a gene encoding GXM3 (contig 28694, FC CBOT vs. TOP, MID and FBOT > 12, 9 and 51, respectively) was actively involved in the xylan methylation.

In the xylan acetylation process, we identified genes encoding two types of proteins with acetyl transferase activity: one is Trichome Birefringence-Like protein, corresponding to *TBL29/ESK1* (*ESKIMO1*, contig 22728), *TBL31* (contig 10608), *TBL33* (contig 26349, 15401, 28271 and 15400) and *TBL34* (contig 33688); another type is Reduced Wall Acetylation protein, i.e., *RWA3* (contig 11578 and 26255). Mutations in these genes, either alone or in combination, showed a significant reduction in the acetyl content of xylan (Lee, Teng, Zhong, & Ye, 2011; Yuan et al., 2016; Yuan, Teng, Zhong and Ye, 2016a, 2016b). It is interesting to note that a similar battery of xylan-biosynthetic genes was highly expressed in mature hemp hypocotyls (20 days after sowing; Behr et al., 2016), as well as in the bast fibres separated from internodes containing the snap point (Guerriero, Behr, Legay, et al., 2017). It was suggested that this phenomenon could be associated with the deposition of xylan in the outermost layer of hemp bast fibres, as was evidenced by the immunodetection of xylan (Behr et al., 2016). Together with the immunohistochemical analyses (Figure S1), the transcriptomic data presented here reflect the possible absence of xylan in the nettle bast fibres, which may explain the silkier feature of these fibres with respect to those extracted from textile hemp.

Pectin biosynthesis in the CBOT is evidenced by the high expression of genes encoding UGD2 (UDP-glucose 6-dehydrogenase 2, contig 15115 and 13912) and UGD3 (contig 10987 and 891), which play a key role in producing UDP-glucuronic acid and, therefore, pectic polysaccharides (Reboul et al., 2011).

Similarly to C3, C4 shows a clear induction of genes partaking in lignin biosynthesis in the CBOT, including the essential steps to produce the building blocks, namely aromatic amino acid family biosynthesis and its downstream phenylpropanoid biosynthetic pathway. The presence of lignin in the CBOT was also visualized/quantified by histochemical and chemical analyses (Backes et al., 2018). Interestingly, genes associated with "lignan biosynthetic process" are highly expressed in the CBOT. For example, *DIR6* (dirigent protein 6, contig 24527) displays a 4-fold increase in CBOT as compared to TOP or MID and 18-fold increase with respect to FBOT. This finding indicates that clone 13 may produce high amount of lignans, which is of industrial interest, since plant lignans have numerous biological effects in mammals, such as antitumor, antioxidant and antiprostatic activities (Kim et al., 2009). A thorough metabolic profiling of nettle clone 13 would shed more light on this. In previous studies, lignans were detected in nettle roots (Kraus & Spiteller, 1990) and their potential beneficial effect on benign prostatic hyperplasia was reported (Schöttner, Gansser, & Spiteller, 1997).

The presence of a regulatory network of SCW formation is further supported by the high expression of the master regulator *VND1* (vascular-related NAC domain 1, contig 24094) (Zhou, Zhong, & Ye, 2014), accompanied by the second-layer master switch *MYB46* (contig 28627) (Zhong, Richardson, & Ye, 2007) and its downstream TFs, namely *MYB43* (contig 12554), *MYB54* (contig 24665) and *MYB103* (contig 30826; Zhong, Lee, Zhou, McCarthy, & Ye, 2008). Interestingly, *MYB46* was previously reported to be highly expressed in the hemp bast fibres at the snap point to regulate SCW biogenesis (Guerriero, Behr, Legay, et al., 2017).

3.6 | GOE analysis of the internodes at the top and middle

The GOs of the top and middle internodes are represented by cluster C5 and C6. The differences in the expression patterns between these clusters are the progressive decrease from the top to the FBOT in C5, as opposed to the sharp difference existing in the top and middle internodes with respect to the FBOT and CBOT samples in C6 (Data S1). In C5, ontologies related to jasmonic acid (JA) biosynthetic process and, more in general, to fatty acid-derived compounds, are present, together with genes partaking in flavonoid and indole-containing compound metabolic processes. Additionally, ontologies related with lignin biosynthesis, sterol metabolic process, cutin/cuticle development, systemic acquired resistance are present. More general processes appear too, notably carboxylic acid catabolic processes, response to karrikin and drug transport.

The JA-related processes are linked with the response to wounding, an important aspect when considering actively elongating internodes. Bast fibres indeed show a typical intrusive/invasive mode of growth (Ageeva et al., 2005; Gorshkova et al., 2012; Guerriero et al., 2013; Lev-Yadun, 2010; Snegireva et al., 2010) which likely involves the perception of signals by neighboring parenchymatic cells (Berni, Luyckx, et al., 2018). The penetration of the middle lamellas is an event triggering wounding, but no callose deposition was observed in flax (Snegireva et al., 2010). However, a role of JA in intrusive growth cannot be excluded at this stage. Allene oxide synthase (AOS) is the first enzyme intervening in the synthesis of JA (Mueller, 1997; Sivasankar, Sheldrick, & Rothstein, 2000). In our dataset *AOS* (*At5 g42650*) (represented by contigs 24544 and 26032) is expressed at the highest levels in the internodes at the top (expression ratios TOP *vs* FBOT > 3 for both contigs and TOP vs. CBOT > 65 for contig 24544 and >35 for contig 26032). Other genes intervening in JA biosynthesis are *LOX1*, *LOX2* (*At3g45140*) and *JMT* (*At1g19640*) and appear in C5. *LOX1* shows a FC TOP *vs* CBOT > 6, MID vs. CBOT > 3, FBOT vs. CBOT > 5. *LOX2* is represented by four contigs (contig_16075, contig_16077, contig_32893 and contig_16844), with a FC TOP vs. CBOT > 10 for all of the *LOX2* contigs. JMT, which catalyses the formation of methyl jasmonate, an important volatile compound signalling defence response (Jang et al., 2014; Seo et al., 2001), is expressed highly in the TOP and MID internodes (FC > 3 with respect to CBOT). However, this gene is expressed at high levels

also in FBOT, where it may be involved in senescing processes (Wilmowicz et al., 2016), which are ongoing in older regions of the stems.

C5 is also characterized by genes involved in auxin and indole-containing compound metabolic process (Data S1). These ontologies are linked to peroxisomal β-oxidations, as well as flavonoid biosynthetic processes, which are both represented in C5. Conversion of indole-3-butyric acid (IBA) to indole-3-acetic acid (IAA) and vice versa is known (Tognetti et al., 2010) and the higher expression of *IBR1*, together with *UGT74E2* in the TOP, MID and FBOT internodes is indicative of the presence of an IBA-related network.

IBA is converted to IAA via reactions resembling peroxisomal β-oxidation processes (Strader, Culler, Cohen, & Bartel, 2010) and it represents an auxin storage form. The endogenous pool of active auxin needs to be tightly controlled during plant development via IAA conjugation, as well as IAA-IBA interconversion. The ontologies related to indole-containing compounds and peroxisomal fatty acid oxidation suggest the presence of a mechanism controlling the concentration of active auxin in younger internodes via the conversion of IBA to IAA. The gene *IBR1* is indeed expressed > 14 fold at the MID, and >21 fold in young elongating internodes at the TOP, as compared to the CBOT (Data S1). *IBR1* encodes an enzyme belonging to the short-chain dehydrogenase/reductase family and *ibr1* mutants display reduced lateral root initiation and reduced inhibition of root elongation in response to IBA (Zolman, Martinez, Millius, Adham, & Bartel, 2008). Interestingly, the gene *UGT74E2* is also expressed at the highest levels at the TOP: it encodes a UDP-glucosyltransferase acting on IBA and responsible for its conversion to IBA-Glc (Tognetti et al., 2010). *Arabidopsis* plants overexpressing this gene show alterations in auxin homeostasis, with an induction of IAA oxidative pathways and phenotypic anomalies, namely more compact rosettes with shorter petioles and darker leaves, decreased height, together with enhanced shoot branching (Tognetti et al., 2010). IBA and IBA-Glc homeostasis may therefore play a role in the correct development of young nettle internodes. A fine molecular mechanism is here highlighted, in which glucosylation of IBA on one hand and conversion of IBA to IAA constitute part of this regulation.

The presence of an auxin-driven mechanism in elongating stem internodes requires a further level of control linked with the reduction of oxidative stress (Peer, Cheng, & Murphy, 2013). The formation of IAA engenders reactive oxygen species (ROS) which are known to be involved in fibre elongation (recently reviewed by (Berni, Luyckx, et al., 2018). Their role as a "double-edged sword" means that while they ensure the correct execution of developmental processes, their presence within plant cells needs to be strictly controlled, to avoid undesired oxidative damages to biological structures and macromolecules. Flavonoids are well-known scavengers of ROS (Berni, Cantini, et al., 2018) and this capacity is linked to the structural features (geometry of the molecule, number and position of –OH groups) of this large class of polyphenolic plant secondary metabolites. In the dataset here obtained, an increased expression of genes partaking in flavonoid biosynthesis is evident at the TOP and MID: the transcripts encoding *CHIL* (*chalcone isomerase-like*),

TT4 (*CHS, chalcone synthase*), *TT5* (*CHI, chalcone isomerase*) and *TT7* (*F3′H, flavonoid 3′-hydroxylase*) show high expression in young internodes, with a peak at the MID (Data S1). The expression is also high in the FBOT, suggesting an active secondary metabolism in the cortical tissues of nettle stems. It is interesting to note, in this respect, that in young elongating fibres of hemp the "flavonoid biosynthetic process" ontology was also enriched (Guerriero, Behr, Legay, et al., 2017). The genes *TT4*, *TT5*, *TT7* are all classified as "early genes" in the flavonoid biosynthetic pathway (Bashandy, Taconnat, Renou, Meyer, & Reichheld, 2009) and working in concert for the synthesis of dihydroflavonols. The product of *CHIL* was shown to intervene at the same step as TT5-CHI and to co-express, co-localize in the endoplasmic reticulum and possibly to interact with it in thale cress (Jiang et al., 2015) for the production of flavonoids. CHIL has no catalytic activity when produced recombinantly and may function as a chaperone or enhancer favouring the production of flavonoids (Jiang et al., 2015). The role of flavonoids in nettle stem could also involve the regulation of polar auxin transport: these secondary metabolites and, particularly, those synthesized by the action of the "early" flavonoid biosynthetic genes (kaempferol, quercetin), negatively regulate auxin transport and cause localized accumulation of the phytohormone (Peer & Murphy, 2007). Both direct and indirect interactions can explain the flavonoids-regulated auxin transport: for example they can modulate membrane fluidity, as well phosphorylation (Peer & Murphy, 2007). At this stage, it is not possible to ascertain if the role of flavonoids in nettle stem development is preferentially associated with ROS scavenging, rather than modulation of auxin transport, although the rapid elongation of bast fibres and their intrusive growth mechanism would indicate ROS production (Berni, Luyckx, et al., 2018).

A gene orthologous to thale cress *DTX35* shows highest expression at the MID (MID vs. CBOT > 30): recently, the product of this gene was shown to regulate turgor pressure in e.g., rapidly elongating cells such as the pollen tube, by functioning as tonoplast-localized chloride channel (Zhang, Zhao, et al., 2017). Interestingly, the product of the same gene was previously shown to mediate flavonoid transport and mutants displayed slightly reduced anthocyanin levels and were affected in fertility (Thompson, Wilkins, Demidchik, Davies, & Glover, 2010).

A further indication of the potential implication of flavonoids in ROS scavenging comes from the GOE analysis of C6: genes involved in ROS biosynthetic processes are present, as well as flavonoid biosynthesis (Data S1). The gene coding for the TF MYB113 involved in anthocyanin biosynthesis is expressed at the highest levels in the TOP (TOP vs. FBOT > 40): this indicates pigment synthesis for photoprotective purpose. Another gene coding for a central TF is *MYC2* (TOP vs. FBOT/CBOT > 4; Data S1): this is a master regulator of the jasmonic acid response and it positively regulates flavonoid biosynthesis (Kazan & Manners, 2013). In support of the above-described genes involved in the auxin-linked peroxisomal β-oxidative processes, *HAOX1* (*hydroxyl acid oxidase*) is present in C6 (TOP vs. FBOT > 2 and TOP vs. CBOT > 15; Data S1). This gene belongs to the *GOX* (*glycolate oxidase*) family (Rojas et al., 2012) and indicates an active peroxisomal

metabolism in young nettle stem regions. Peroxisomes are metabolic "hubs" supplying important intermediates used e.g., for the synthesis of phytohormones (Nyathi & Baker, 2006) and generate H_2O_2 during oxidative reactions. Another gene involved in ROS formation is *RPH1* (*resistance to Phytophthora 1*; TOP vs. FBOT > 2 and TOP vs. CBOT > 4; Data S1) encoding a chloroplast protein positively regulating oomycete pathogen-induced oxidative burst (Belhaj, Lin, & Mauch, 2009). Finally, in the ROS-related ontology, there is also *NIA2* (*nitrate reductase 2*) corresponding to contigs 4943 and 4092 (TOP vs. FBOT > 3 and TOP vs. CBOT > 5 for contig 4943, TOP vs. FBOT > 2 and TOP vs. CBOT > 3.5 for contig 4092; Data S1). NIA2 is responsible for nitric oxide (NO) formation during ABA-driven stomatal closure (Desikan, Griffiths, Hancock, & Neill, 2002) and is recognized as an important source of this signalling molecule (Chamizo-Ampudia, Sanz-Luque, Llamas, Galvan, & Fernandez, 2017). NO was shown to determine pollen tube growth and re-orientation (Prado, Porterfield, & Feijó, 2004) and therefore has a role in regulating the development of fast elongating cells. This is particularly interesting in fibre crops, since bast fibres, despite not displaying a tip-growth modality, are nevertheless fast growing cells. Investigating the role of NO in bast fibre development is an interesting topic for future studies.

In C6, genes involved in expansion are likewise present, with the expansin genes *EXPA1-8-15* upregulated at the TOP/MID (TOP vs. FBOT > 16 and TOP vs. CBOT > 4.5 for *EXPA8* and *15*; Data S1). This confirms the rapid elongation of tissues sampled from young internodes.

3.7 | Targeted quantification of phenolic compounds

The transcriptomic signature of C5 and C6 highlights the presence of an enrichment in ontologies related to flavonoid biosynthesis. Therefore, a targeted quantification of some flavonoids was performed in order to see whether the higher expression of flavonoid biosynthetic genes results in higher amounts of flavonoids in young internodes. The flavonols quercetin, kaempferol and isorhamnetin were targeted, as they were reported to be abundant in nettle (Farag, Weigend, Luebert, Brokamp, & Wessjohann, 2013), together with catechins, rutin and vanillic acid. Isorhamnetin could only be detected in the TOP and MID internodes (with the TOP showing statistically significant higher values than the MID with the Student's *t*-test), while kaempferol is present in the MID and peels at the bottom (the MID content is statistically significant higher than the FBOT with at the Student's *t*-test; Figure 4). The highest abundance of flavonoids is observed in the MID internode, a finding corroborating the transcriptomic analysis. It is interesting to note that, while at the gene level both the TOP and MID have a high expression of genes involved in flavonoid biosynthesis, the metabolite quantification reveals a spatial shift, with the MID and FBOT showing the highest values. A delay between gene expression and metabolite production is indicative of a temporal gap necessary to synthesize the related enzymes and accumulate the metabolites. It will be interesting to address the reasons of this shift, especially if one considers the post-translational regulatory mechanism recently highlighted in thale cress and comprising a Kelch domain-containing protein (Zhang, Abrahan,

FIGURE 4 Quantification of flavonoids in the nettle internodes expressed as µg per g of dry weight (DW). The number of biological replicates (*n*) is 4, with three technical replicates. Letters (a–d) indicate statistically significant differences between groups (*p* < 0.05) at the one-way ANOVA with Tukey's post-hoc test. The asterisks indicate statistically significant values (*p* < 0.05, Student's *t*-test)
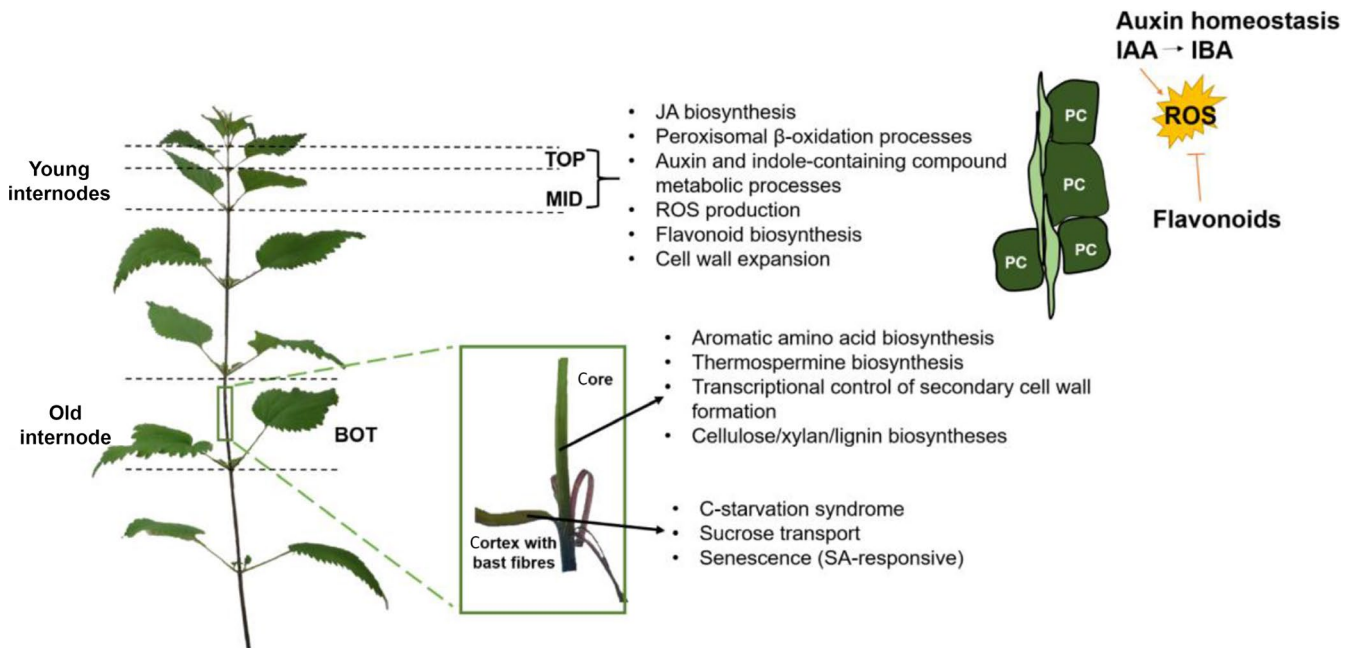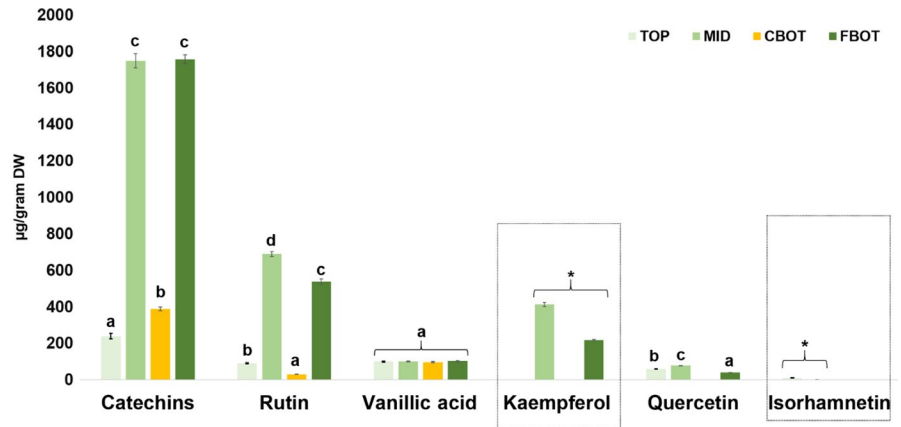

FIGURE 5 Schematic model showing the key processes occurring at each stem internode/tissue analysed. The cartoon on the right hand-side refers to a longitudinal view of intrusively growing bast fibres. Young internodes in intrusive growth (TOP/MID) are characterized by cell wall expansion and jasmonic acid (JA) biosynthesis, probably due to the signal perceived by neighboring parenchyma cells (PC). An active auxin metabolism is also observed, with peroxisomal β-oxidation processes linked to the conversion IAA to IBA. ROS are thus produced, whose effects are mitigated by flavonoids. Flavonoid biosynthetic genes are indeed highly expressed in young internodes and flavonoids are high in amount at the MID. The core tissues at the BOT have a predominance of ontologies related to secondary cell wall formation and xylan/cellulose/lignin deposition. A gene related to thermospermine biosynthesis is also highly expressed in the core, where it controls xylem differentiation. In the fibre-rich tissues at the BOT, ontologies related to the C starvation syndrome are evident, because of the sucrose demand and UDP-glucose need for bast fibre thickening. Senescence processes, known to be controlled by salicylic acid (SA), are also observed

Colquhoun, & Liu, 2017). Posttranslational event may be responsible for this shift in metabolite production in the nettle internodes.

4 | CONCLUSIONS

In this study, we provide a draft transcriptome of a nettle fibre clone and analyse for the first time the gene dynamics along the stem from a cell wall perspective. We reveal a unique transcriptomic "fingerprint" of elongating and older nettle internodes. In particular, we

unveil the presence of a network involving ROS formation and genes involved in phytohormone and secondary metabolite biosynthesis in young internodes with elongating bast fibres. Tissues containing bast fibres sampled from older stem regions are characterised by a molecular network involving the C starvation syndrome, most likely resulting from the need of UDP-glucose required for bast fibre thickening. A model summarising the main events in young and older internodes is given in Figure 5.

The cell wall analysis reveals some interesting features in relation to rhamnogalacturonan composition of cortical tissues from older

internodes, while the histochemical analysis shows the absence of xylan from the S1-layer of bast fibres, differently from what reported in hemp (Chernova et al., 2018). Our results will be important for future molecular analysis on nettle, a neglected, yet promising multi-purpose fibre crop.

CONFLICT OF INTERESTS

The authors declare no conflict of interest associated with the work described in this manuscript.

AUTHOR CONTRIBUTIONS

XX performed immunohistochemistry with LM10, cell wall sequential extraction and wrote the results on confocal microscopy, chemical analysis of the cell walls and cluster 4 of the RNA-Seq data. BA grew the plants, sampled the tissues, performed RNA extraction, primer design and validation, RNA-Seq analysis and RT-qPCR. LS contributed to the bioinformatics analysis. BR performed the quantification of phenolic compounds. CG and FC performed TEM analysis. GE propagated and supplied the nettle clone and provided an optimized protocol for the growth conditions of the stem cuttings. XX, BA, LS, HJ-F, GE, CG critically read the manuscript and helped in data interpretation. GG conceived the idea of the study, designed the experiment, performed library preparation and RNA-Seq, carried out the bioinformatics analyses, interpreted the data, wrote the paper and leads the project CABERNET.

REFERENCES

Ageeva, M. V., Petrovská, B., Kieft, H., Sal'nikov, V. V., Snegireva, A. V., van Dam, J. E., ... van Lammeren, A. A. (2005). Intrusive growth of flax phloem fibers is of intercalary type. *Planta*, *222*, 565–574.

Al-Ani, L., & Deyholos, M. K. (2018). Transcriptome assembly of the bast fiber crop, Ramie, *Boehmeria nivea* (L.) Gaud. (Urticaceae). *Fibers*, *6*, 8.

Bacci, L., Baronti, S., Predieri, S., & di Virgilio, N. (2009). Fiber yield and quality of fiber nettle (*Urtica dioica* L.) cultivated in Italy. *Industrial Crops and Products*, *29*, 480–484.

Backes, A., Behr, M., Xu, X., Gatti, E., Legay, S., Predieri, S., ... Guerriero, G. (2018). Sucrose synthase gene expression analysis in the fibre nettle (*Urtica dioica* L.) cultivar "clone 13". *Industrial Crops and Products*, *123*, 315–322.

Baima, S., Forte, V., Possenti, M., Peñalosa, A., Leoni, G., Salvi, S., ... Morelli, G. (2014). Negative feedback regulation of auxin signaling by ATHB8–ACL5–BUD2 transcription module. *Molecular Plant*, *7*, 1006–1025.

Bashandy, T., Taconnat, L., Renou, J.-P., Meyer, Y., & Reichheld, J.-P. (2009). Accumulation of flavonoids in an ntra ntrb mutant leads to tolerance to UV-C. *Molecular Plant*, *2*, 249–258.

Behr, M., Legay, S., Žižková, E., Motyka, V., Dobrev, P. I., Hausman, J.-F., ... Guerriero, G. (2016). Studying secondary growth and bast fiber development: The Hemp Hypocotyl Peeks behind the Wall. *Frontiers in Plant Science*, *7*, 1733.

Belhaj, K., Lin, B., & Mauch, F. (2009). The chloroplast protein RPH1 plays a role in the immune response of *Arabidopsis* to *Phytophthora brassicae*. *Plant Journal for Cell and Molecular Biology*, *58*, 287–298.

Berni, R., Cantini, C., Romi, M., Hausman, J.-F., Guerriero, G., & Cai, G. (2018). Agrobiotechnology goes wild: Ancient local varieties as sources of bioactives. *International Journal of Molecular Sciences*, *19*, 2248.

Berni, R., Luyckx, M., Xu, X., Legay, S., Sergeant, K., Hausman, J.-F., ... Guerriero, G. (2018). Reactive oxygen species and heavy metal stress in plants: Impact on the cell wall and secondary metabolism. *Environmental and Experimental Botany*, *161*, 98–106.

Berni, R., Romi, M., Parrotta, L., Cai, G., & Cantini, C. (2018). Ancient tomato (*Solanum lycopersicum* L.) varieties of tuscany have high contents of bioactive compounds. *Horticulturae*, *4*, 51.

Bindea, G., Mlecnik, B., Hackl, H., Charoentong, P., Tosolini, M., Kirilovsky, A., ... Galon, J. (2009). ClueGO: a Cytoscape plug-in to decipher functionally grouped gene ontology and pathway annotation networks. *Bioinformatics*, *25*, 1091–1093.

Burmistrova, N. A., Krasavina, M. S., & Akanov, E. N. (2009). Salicylic acid can regulate phloem unloading in the root tip. *Russian Journal of Plant Physiology*, *56*, 627–634.

Carruthers, M., Yurchenko, A. A., Augley, J. J., Adams, C. E., Herzyk, P., & Elmer, K. R. (2018). *De novo* transcriptome assembly, annotation and comparison of four ecological and evolutionary model salmonid fish species. *BMC Genomics*, *19*, 32.

Chamizo-Ampudia, A., Sanz-Luque, E., Llamas, A., Galvan, A., & Fernandez, E. (2017). Nitrate reductase regulates plant nitric oxide homeostasis. *Trends in Plant Science*, *22*, 163–174.

Chen, L.-Q., Lin, I. W., Qu, X.-Q., Sosso, D., McFarlane, H. E., Londoño, A., ... Frommer, W. B. (2015). A cascade of sequentially expressed sucrose transporters in the seed coat and endosperm provides nutrition for the *Arabidopsis* Embryo. *Plant Cell*, *27*, 607–619.

Chernova, T. E., Mikshina, P. V., Salnikov, V. V., Ibragimova, N. N., Sautkina, O. V., & Gorshkova, T. A. (2018). Development of distinct cell wall layers both in primary and secondary phloem fibers of hemp (*Cannabis sativa* L.). *Industrial Crops and Products*, *117*, 97–109.

Crônier, D., Monties, B., & Chabbert, B. (2005). Structure and chemical composition of bast fibers isolated from developing hemp stem. *Journal of Agriculture and Food Chemistry*, *53*, 8279–8289.

Curtis, T. Y., Bo, V., Tucker, A., & Halford, N. G. (2018). Construction of a network describing asparagine metabolism in plants and its application to the identification of genes affecting asparagine metabolism in wheat under drought and nutritional stress. *Food and Energy Security*, *7*, e00126.

Desikan, R., Griffiths, R., Hancock, J., & Neill, S. (2002). A new role for an old enzyme: Nitrate reductase-mediated nitric oxide generation is required for abscisic acid-induced stomatal closure in *Arabidopsis thaliana*. *Proceedings of the National Academy of Sciences of the United States of America*, *99*, 16314–16318.

Ding, L., Pandey, S., & Assmann, S. M. (2008). *Arabidopsis* extra-large G proteins (XLGs) regulate root morphogenesis. *Plant Journal*, *53*, 248–263.

Eisen, M. B., Spellman, P. T., Brown, P. O., & Botstein, D. (1998). Cluster analysis and display of genome-wide expression patterns. *Proceedings of the National Academy of Sciences of the United States of America*, *95*, 14863–14868.

Farag, M. A., Weigend, M., Luebert, F., Brokamp, G., & Wessjohann, L. A. (2013). Phytochemical, phylogenetic, and anti-inflammatory evaluation of 43 *Urtica* accessions (stinging nettle) based on UPLC-Q-TOF-MS metabolomic profiles. *Phytochemistry*, *96*, 170–183.

Fukunaga, S., Sogame, M., Hata, M., Singkaravanit-Ogawa, S., Piślewska-Bednarek, M., Onozawa-Komori, M., … Takano, Y. (2017). Dysfunction of *Arabidopsis* MACPF domain protein activates programmed cell death via tryptophan metabolism in MAMP-triggered immunity. *Plant Journal*, *89*, 381–393.

Gatti, E., Di Virgilio, N., & Bacci, L. (2008). Development of propagation methods for organic production of fibre (*Urtica dioica L.*). In *International Conference on Flax and Other Bast Plants*.

Ge, S. X., Son, E. W., & Yao, R. (2018). iDEP: An integrated web application for differential expression and pathway analysis of RNA-Seq data. *BMC Bioinformatics*, *19*, 534.

Gonzali, S., Loreti, E., Solfanelli, C., Novi, G., Alpi, A., & Perata, P. (2006). Identification of sugar-modulated genes and evidence for in vivo sugar sensing in *Arabidopsis*. *Journal of Plant Research*, *119*, 115–123.

Gorshkov, O., Mokshina, N., Gorshkov, V., Chemikosova, S., Gogolev, Y., & Gorshkova, T. (2017). Transcriptome portrait of cellulose-enriched flax fibres at advanced stage of specialization. *Plant Molecular Biology*, *93*, 431–449.

Gorshkova, T., Brutch, N., Chabbert, B., Deyholos, M., Hayashi, T., Lev-Yadun, S., … Pilate, G. (2012). Plant fiber formation: State of the Art, recent and expected progress, and open questions. *Critical Reviews in Plant Sciences*, *31*, 201–228.

Gorshkova, T. A., Chemikosova, S. B., Sal'nikov, V. V., Pavlencheva, N. V., Gur'janov, O. P., Stolle-Smits, T., & van Dam, J. E. G. (2004). Occurrence of cell-specific galactan is coinciding with bast fiber developmental transition in flax. *Industrial Crops and Products*, *19*, 217–224.

Goubet, F., Bourlard, T., Girault, R., Alexandre, C., Vandevelde, M.-C., & Morvan, C. (1995). Structural features of galactans from flax fibres. *Carbohydrate Polymers*, *27*, 221–227.

Guerriero, G., Behr, M., Backes, A., Faleri, C., Hausman, J.-F., Lutts, S., & Cai, G. (2017). Bast fibre formation: Insights from next-generation sequencing. *Procedia Engineering*, *200*, 229–235.

Guerriero, G., Behr, M., Legay, S., Mangeot-Peter, L., Zorzan, S., Ghoniem, M., & Hausman, J.-F. (2017). Transcriptomic profiling of hemp bast fibres at different developmental stages. *Scientific Reports*, *7*, 4961.

Guerriero, G., Mangeot-Peter, L., Legay, S., Behr, M., Lutts, S., Siddiqui, K. S., & Hausman, J.-F. (2017). Identification of fasciclin-like arabinogalactan proteins in textile hemp (*Cannabis sativa* L.): *In silico* analyses and gene expression patterns in different tissues. *BMC Genomics*, *18*, 741.

Guerriero, G., Sergeant, K., & Hausman, J.-F. (2013). Integrated -Omics: A powerful approach to understanding the heterogeneous lignification of fibre crops. *International Journal of Molecular Sciences*, *14*, 10958–10978.

Haas, B. J., Papanicolaou, A., Yassour, M., Grabherr, M., Blood, P. D., Bowden, J., … Regev, A. (2013). *De novo* transcript sequence reconstruction from RNA-Seq: Reference generation and analysis with Trinity. *Nature Protocols*, *8*, 1494–1512.

Hanzawa, Y., Takahashi, T., Michael, A. J., Burtin, D., Long, D., Pineiro, M., … Komeda, Y. (2000). *ACAULIS5*, an *Arabidopsis* gene required for stem elongation, encodes a spermine synthase. *EMBO Journal*, *19*, 4248–4256.

Hartl, A., & Vogl, C. R. (2002). Dry matter and fibre yields, and the fibre characteristics of five nettle clones (*Urtica dioica* L.) organically grown in Austria for potential textile use. *American Journal of Alternative Agriculture*, *17*, 195–200.

Harwood, J., & Edom, G. (2012). Nettle fibre: Its prospects, uses and problems in historical perspective. *Textile History*, *43*, 107–119.

Hellemans, J., Mortier, G., De Paepe, A., Speleman, F., & Vandesompele, J. (2007). qBase relative quantification framework and software for management and automated analysis of real-time quantitative PCR data. *Genome Biology*, *8*, R19.

Hill, J. L., Hammudi, M. B., & Tien, M. (2014). The *Arabidopsis* cellulose synthase complex: A proposed hexamer of CESA trimers in an equimolar stoichiometry. *Plant Cell*, *26*, 4834–4842.

Huang, G.-Q., Gong, S.-Y., Xu, W.-L., Li, W., Li, P., Zhang, C. J., … Li, X. B. (2013). A fasciclin-like arabinogalactan protein, GhFLA1, is involved in fiber initiation and elongation of cotton. *Plant Physiology*, *161*, 1278–1290.

Hummel, M., Rahmani, F., Smeekens, S., & Hanson, J. (2009). Sucrose-mediated translational control. *Annals of Botany*, *104*, 1–7.

Hwang, I. S., An, S. H., & Hwang, B. K. (2011). Pepper asparagine synthetase 1 (CaAS1) is required for plant nitrogen assimilation and defense responses to microbial pathogens. *Plant Journal for Cell and Molecular Biology*, *67*, 749–762.

Jacobs, A., Palm, M., Zacchi, G., & Dahlman, O. (2003). Isolation and characterization of water-soluble hemicelluloses from flax shive. *Carbohydrate Research*, *338*, 1869–1876.

Jang, G., Shim, J. S., Jung, C., Song, J. T., Lee, H. Y., Chung, P. J., … Choi, Y. D. (2014). Volatile methyl jasmonate is a transmissible form of jasmonate and its biosynthesis is involved in systemic jasmonate response in wounding. *Plant Biotechnology Reports*, *8*, 409–419.

Jiang, W., Yin, Q., Wu, R., Zheng, G., Liu, J., Dixon, R. A., & Pang, Y. (2015). Role of a chalcone isomerase-like protein in flavonoid biosynthesis in *Arabidopsis thaliana*. *Journal of Experimental Botany*, *66*, 7165–7179.

Joshi, C. P. (2003). Xylem-specific and tension stress—responsive expression of cellulose synthase genes from aspen trees. In B. H. Davison, J. W. Lee, M. Finkelstein, & J. D. McMillan (Eds.), *Biotechnology for fuels and chemicals: The Twenty-Fourth Symposium*. Applied Biochemistry and Biotechnology (pp. 17–25). Totowa, NJ: Humana Press.

Kakehi, J., Kuwashiro, Y., Niitsu, M., & Takahashi, T. (2008). Thermospermine is required for stem elongation in *Arabidopsis thaliana*. *Plant and Cell Physiology*, *49*, 1342–1349.

Kazan, K., & Manners, J. M. (2013). MYC2: The master in action. *Molecular Plant*, *6*, 686–703.

Kim, H. J., Ono, E., Morimoto, K., Yamagaki, T., Okazawa, A., Kobayashi, A., & Satake, H. (2009). Metabolic engineering of lignan biosynthesis in *Forsythia* cell culture. *Plant and Cell Physiology*, *50*, 2200–2209.

Knott, J. M., Römer, P., & Sumper, M. (2007). Putative spermine synthases from *Thalassiosira pseudonana* and *Arabidopsis thaliana* synthesize thermospermine rather than spermine. *FEBS Letters*, *581*, 3081–3086.

Kraus, R., & Spiteller, G. (1990). Phenolic compounds from roots of *Urtica dioica*. *Phytochemistry*, *29*, 1653–1659.

Kregiel, D., Pawlikowska, E., & Antolak, H. (2018). *Urtica* spp.: Ordinary plants with extraordinary properties. *Molecules: A Journal of Synthetic Chemistry and Natural Product Chemistry*, *23*, 1664.

Lam, H. M., Hsieh, M. H., & Coruzzi, G. (1998). Reciprocal regulation of distinct asparagine synthetase genes by light and metabolites in *Arabidopsis thaliana*. *Plant Journal for Cell and Molecular Biology*, *16*, 345–353.

Lee, C., Teng, Q., Zhong, R., & Ye, Z.-H. (2011). The four *Arabidopsis REDUCED WALL ACETYLATION* genes are expressed in secondary wall-containing cells and required for the acetylation of xylan. *Plant and Cell Physiology*, *52*, 1289–1301.

Lee, C., Teng, Q., Zhong, R., & Ye, Z.-H. (2012). *Arabidopsis* GUX proteins are glucuronyltransferases responsible for the addition of glucuronic acid side chains onto xylan. *Plant and Cell Physiology*, *53*, 1204–1216.

Lee, C., Teng, Q., Zhong, R., Yuan, Y., Haghighat, M., & Ye, Z.-H. (2012). Three *Arabidopsis* DUF579 domain-containing GXM proteins are methyltransferases catalyzing 4-*O*-methylation of glucuronic acid on xylan. *Plant and Cell Physiology*, *53*, 1934–1949.

Lev-Yadun, S. (2010). Plant fibers: Initiation, growth, model plants, and open questions. *Russian Journal of Plant Physiology*, *57*, 305–315.

Li, J., Brader, G., Kariola, T., & Palva, E. T. (2006). WRKY70 modulates the selection of signaling pathways in plant defense. *Plant Journal*, *46*, 477–491.

Li, Y. Q., Chen, F., Linskens, H. F., & Cresti, M. (1994). Distribution of un-esterified and esterified pectins in cell walls of pollen tubes of flowering plants. *Sexual Plant Reproduction*, 7, 145–152.

Liu, K., Sun, J., Yao, L., & Yuan, Y. (2012). Transcriptome analysis reveals critical genes and key pathways for early cotton fiber elongation in Ligon lintless-1 mutant. *Genomics*, 100, 42–50.

Mangeot-Peter, L., Legay, S., Hausman, J.-F., Esposito, S., & Guerriero, G. (2016). Identification of reference genes for RT-qPCR data normalization in *Cannabis sativa* stem tissues. *International Journal of Molecular Sciences*, 17, E1556.

Miller, J. D., Arteca, R. N., & Pell, E. J. (1999). Senescence-associated gene expression during ozone-induced leaf senescence in *Arabidopsis*. *Plant Physiology*, 120, 1015–1024.

Morris, K., Mackerness, S., Page, T., John, C. F., Murphy, A. M., Carr, J. P., & Buchanan Wollaston, V. (2000). Salicylic acid has a role in regulating gene expression during leaf senescence. *Plant Journal*, 23, 677–685.

Mortazavi, A., Williams, B. A., McCue, K., Schaeffer, L., & Wold, B. (2008). Mapping and quantifying mammalian transcriptomes by RNA-Seq. *Nature Methods*, 5, 621–628.

Moschou, P. N., & Roubelakis-Angelakis, K. A. (2014). Polyamines and programmed cell death. *Journal of Experimental Botany*, 65, 1285–1296.

Mueller, M. J. (1997). Enzymes involved in jasmonic acid biosynthesis. *Physiologia Plantarum*, 100, 653–663.

Muñiz, L., Minguet, E. G., Singh, S. K., Pesquet, E., Vera-Sirera, F., Moreau-Courtois, C. L., … Tuominen, H. (2008). ACAULIS5 controls *Arabidopsis xylem* specification through the prevention of premature cell death. *Development*, 135, 2573–2582.

Nairn, C. J., & Haselkorn, T. (2005). Three loblolly pine *CesA* genes expressed in developing xylem are orthologous to secondary cell wall *CesA* genes of angiosperms. *New Phytologist*, 166, 907–915.

Nakano, Y., Yamaguchi, M., Endo, H., Rejab, N. A., & Ohtani, M. (2015). NAC-MYB-based transcriptional regulation of secondary cell wall biosynthesis in land plants. *Frontiers in Plant Science*, 6, 288.

Nyathi, Y., & Baker, A. (2006). Plant peroxisomes as a source of signalling molecules. *Biochimica et Biophysica Acta*, 1763, 1478–1495.

Peer, W. A., Cheng, Y., & Murphy, A. S. (2013). Evidence of oxidative attenuation of auxin signalling. *Journal of Experimental Botany*, 64, 2629–2639.

Peer, W. A., & Murphy, A. S. (2007). Flavonoids and auxin transport: Modulators or regulators? *Trends in Plant Science*, 12, 556–563.

Pelloux, J., Rustérucci, C., & Mellerowicz, E. J. (2007). New insights into pectin methylesterase structure and function. *Trends in Plant Science*, 12, 267–277.

Peña, M. J., Zhong, R., Zhou, G.-K., Richardson, E. A., O'Neill, M. A., Darvill, A. G., … Ye, Z.-H. (2007). *Arabidopsis irregular xylem8* and *irregular xylem9*: Implications for the complexity of glucuronoxylan biosynthesis. *Plant Cell*, 19, 549–563.

Pettolino, F. A., Walsh, C., Fincher, G. B., & Bacic, A. (2012). Determining the polysaccharide composition of plant cell walls. *Nature Protocols*, 7, 1590–1607.

Prado, A. M., Porterfield, D. M., & Feijó, J. A. (2004). Nitric oxide is involved in growth regulation and re-orientation of pollen tubes. *Development*, 131, 2707–2714.

Reboul, R., Geserick, C., Pabst, M., Frey, B., Wittmann, D., Lütz-Meindl, U., … Tenhaken, R. (2011). Down-regulation of UDP-glucuronic acid biosynthesis leads to swollen plant cell walls and severe developmental defects associated with changes in pectic polysaccharides. *Journal of Biological Chemistry*, 286, 39982–39992.

Roach, M. J., & Deyholos, M. K. (2007). Microarray analysis of flax (*Linum usitatissimum* L.) stems identifies transcripts enriched in fibre-bearing phloem tissues. *Molecular Genetics and Genomics*, 278, 149–165.

Roach, M. J., & Deyholos, M. K. (2008). Microarray analysis of developing flax hypocotyls identifies Novel transcripts correlated with

specific stages of phloem fibre differentiation. *Annals of Botany*, 102, 317–330.

Rojas, C. M., Senthil-Kumar, M., Wang, K., Ryu, C.-M., Kaundal, A., & Mysore, K. S. (2012). Glycolate oxidase modulates reactive oxygen species-mediated signal transduction during nonhost resistance in *Nicotiana benthamiana* and *Arabidopsis*. *Plant Cell*, 24, 336–352.

Ruprecht, C., Bartetzko, M. P., Senf, D., Dallabernadina, P., Boos, I., Andersen, M. C. F., … Pfrengle, F. (2017). A synthetic glycan microarray enables epitope mapping of plant cell wall glycan-directed antibodies. *Plant Physiology*, 175, 1094–1104.

Samuga, A., & Joshi, C. P. (2002). A new cellulose synthase gene (*PtrCesA2*) from aspen xylem is orthologous to *Arabidopsis AtCesA7* (irx3) gene associated with secondary cell wall synthesis. *Gene*, 296, 37–44.

Schöttner, M., Gansser, D., & Spiteller, G. (1997). Lignans from the roots of *Urtica dioica* and their metabolites bind to human sex hormone binding globulin (SHBG). *Planta Medica*, 63, 529–532.

Selvendran, R. R., & O'Neill, M. A. (1987). Isolation and analysis of cell walls from plant material. *Methods of Biochemical Analysis*, 32, 25–153.

Seo, P. J., Park, J.-M., Kang, S. K., Kim, S.-G., & Park, C.-M. (2011). An *Arabidopsis* senescence-associated protein SAG29 regulates cell viability under high salinity. *Planta*, 233, 189–200.

Seo, H. S., Song, J. T., Cheong, J.-J., Lee, Y.-H., Lee, Y.-W., Hwang, I., … Choi, Y. D. (2001). Jasmonic acid carboxyl methyltransferase: A key enzyme for jasmonate-regulated plant responses. *Proceedings of the National Academy of Sciences of the United States of America*, 98, 4788–4793.

Siedlecka, A., Wiklund, S., Péronne, M.-A., Micheli, F., Lesniewska, J., Sethson, I., … Mellerowicz, E. J. (2008). Pectin methyl esterase inhibits intrusive and symplastic cell growth in developing wood cells of *Populus*. *Plant Physiology*, 146, 554–565.

Sivasankar, S., Sheldrick, B., & Rothstein, S. J. (2000). Expression of allene oxide synthase determines defense gene activation in tomato. *Plant Physiology*, 122, 1335–1342.

Snegireva, A. V., Ageeva, M. V., Amenitskii, S. I., Chernova, T. E., Ebskamp, M., & Gorshkova, T. A. (2010). Intrusive growth of sclerenchyma fibers. *Russian Journal of Plant Physiology*, 57, 342–355.

Strader, L. C., Culler, A. H., Cohen, J. D., & Bartel, B. (2010). Conversion of endogenous Indole-3-Butyric Acid to Indole-3-acetic acid drives cell expansion in *Arabidopsis* seedlings. *Plant Physiology*, 153, 1577–1586.

Tarancón, C., González-Grandío, E., Oliveros, J. C., Nicolas, M., & Cubas, P. (2017). A conserved carbon starvation response underlies bud dormancy in woody and herbaceous species. *Frontiers in Plant Science*, 8, 788.

Taylor, N. G., Howells, R. M., Huttly, A. K., Vickers, K., & Turner, S. R. (2003). Interactions among three distinct CesA proteins essential for cellulose synthesis. *Proceedings of the National Academy of Sciences of the United States of America*, 100, 1450–1455.

Taylor, N. G., Laurie, S., & Turner, S. R. (2000). Multiple cellulose synthase catalytic subunits are required for cellulose synthesis in *Arabidopsis*. *Plant Cell*, 12, 2529–2540.

Taylor, N. G., Scheible, W. R., Cutler, S., Somerville, C. R., & Turner, S. R. (1999). The *irregular xylem3* locus of *Arabidopsis* encodes a cellulose synthase required for secondary cell wall synthesis. *Plant Cell*, 11, 769–780.

Thompson, E. P., Wilkins, C., Demidchik, V., Davies, J. M., & Glover, B. J. (2010). An *Arabidopsis* flavonoid transporter is required for anther dehiscence and pollen development. *Journal of Experimental Botany*, 61, 439–451.

Tognetti, V. B., Van Aken, O., Morreel, K., Vandenbroucke, K., van de Cotte, B., De Clercq, I., … Van Breusegem, F. (2010). Perturbation of Indole-3-Butyric Acid homeostasis by the UDP-glucosyltransferase UGT74E2 modulates *Arabidopsis* architecture and water stress tolerance. *Plant Cell*, 22, 2660–2679.

XU ET AL.

American Society
of Plant Biologists

SEB
SOCIETY FOR EXPERIMENTAL BIOLOGY

WILEY | 17

Tokuşoğlu, Ö., Ünal, M. K., & Yildirim, Z. (2003). HPLC-UV and GC-MS characterization of the flavonol aglycons quercetin, kaempferol, and myricetin in tomato pastes and other tomato-based products. *Acta Chromatographica*, 13, 196–207.

Tzin, V., & Galili, G. (2010). New insights into the shikimate and aromatic amino acids biosynthesis pathways in plants. *Molecular Plant*, 3, 956–972.

Vandesteene, L., López-Galvis, L., Vanneste, K., Feil, R., Maere, S., Lammens, W., ... Van Dijck, P. (2012). Expansive evolution of the TREHALOSE-6-PHOSPHATE PHOSPHATASE gene family in *Arabidopsis*. *Plant Physiology*, 160, 884–896.

Vicré, M., Lerouxel, O., Farrant, J., Lerouge, P., & Driouich, A. (2004). Composition and desiccation-induced alterations of the cell wall in the resurrection plant *Craterostigma wilmsii*. *Physiologia Plantarum*, 120, 229–239.

Wang, H., Jiang, C., Wang, C., Yang, Y., Yang, L., Gao, X., & Zhang, H. (2015). Antisense expression of the fasciclin-like arabinogalactan protein *FLA6* gene in *Populus* inhibits expression of its homologous genes and alters stem biomechanics and cell wall composition in transgenic trees. *Journal of Experimental Botany*, 66, 1291–1302.

Wilmowicz, E., Kućko, A., Frankowski, K., Świdziński, M., Marciniak, K., & Kopcewicz, J. (2016). Methyl jasmonate-dependent senescence of cotyledons in *Ipomoea nil*. *Acta Physiologiae Plantarum*, 38, 222.

Wu, A.-M., Hörnblad, E., Voxeur, A., Gerber, L., Rihouey, C., Lerouge, P., & Marchant, A. (2010). Analysis of the *Arabidopsis* IRX9/IRX9-L and IRX14/IRX14-L pairs of glycosyltransferase genes reveals critical contributions to biosynthesis of the hemicellulose glucuronoxylan. *Plant Physiology*, 153, 542–554.

Wu, L., Joshi, C. P., & Chiang, V. L. (2000). A xylem-specific cellulose synthase gene from aspen (*Populus tremuloides*) is responsive to mechanical stress. *Plant Journal*, 22, 495–502.

Yordanov, Y. S., Regan, S., & Busov, V. (2010). Members of the LATERAL ORGAN BOUNDARIES DOMAIN Transcription factor family are involved in the regulation of secondary growth in *Populus*. *Plant Cell*, 22, 3662–3677.

Yuan, Y., Teng, Q., Zhong, R., Haghighat, M., Richardson, E. A., & Ye, Z.-H. (2016). Mutations of *Arabidopsis TBL32* and *TBL33* affect xylan acetylation and secondary wall deposition. *PLoS ONE*, 11, e0146460.

Yuan, Y., Teng, Q., Zhong, R., & Ye, Z.-H. (2016a). Roles of *Arabidopsis* TBL34 and TBL35 in xylan acetylation and plant growth. *Plant Science*, 243, 120–130.

Yuan, Y., Teng, Q., Zhong, R., & Ye, Z.-H. (2016b). TBL3 and TBL31, Two *Arabidopsis* DUF231 domain proteins, are required for 3- O - Monoacetylation of Xylan. *Plant and Cell Physiology*, 57, 35–45.

Zhang, X., Abrahan, C., Colquhoun, T. A., & Liu, C.-J. (2017). A proteolytic regulator controlling chalcone synthase stability and flavonoid biosynthesis in *Arabidopsis*. *Plant Cell*, 29, 1157–1174.

Zhang, Yaxi, Xu, S., Ding, P., Wang, D., Cheng, Y. T., He, J., ... Zhang, Y. (2010). Control of salicylic acid synthesis and systemic acquired resistance by two members of a plant-specific family of transcription factors. *Proceedings of the National Academy of Sciences of the United States of America*, 107, 18220–18225.

Zhang, H., Zhao, F.-G., Tang, R.-J., Yu, Y., Song, J., Wang, Y., ... Luan, S. (2017). Two tonoplast MATE proteins function as turgor-regulating chloride channels in *Arabidopsis*. *Proceedings of the National Academy of Sciences of the United States of America*, 114, E2036–E2045.

Zheng, Y., Jiao, C., Sun, H., Rosli, H. G., Pombo, M. A., Zhang, P., ... Fei, Z. (2016). iTAK: A program for genome-wide prediction and classification of plant transcription factors, transcriptional regulators, and protein kinases. *Molecular Plant*, 9, 1667–1670.

Zhong, R., Lee, C., Zhou, J., McCarthy, R. L., & Ye, Z.-H. (2008). A battery of transcription factors involved in the regulation of secondary cell wall biosynthesis in *Arabidopsis*. *Plant Cell*, 20, 2763–2782.

Zhong, R., Richardson, E. A., & Ye, Z.-H. (2007). The MYB46 transcription factor is a direct target of SND1 and regulates secondary wall biosynthesis in *Arabidopsis*. *Plant Cell*, 19, 2776–2792.

Zhou, J., Zhong, R., & Ye, Z.-H. (2014). *Arabidopsis* NAC domain proteins, VND1 to VND5, are transcriptional regulators of secondary wall biosynthesis in vessels. *PLoS ONE*, 9, e105726.

Zolman, B. K., Martinez, N., Millius, A., Adham, A. R., & Bartel, B. (2008). Identification and characterization of *Arabidopsis* Indole-3-butyric acid response mutants defective in Novel peroxisomal enzymes. *Genetics*, 180, 237–251.

SUPPORTING INFORMATION

Additional supporting information may be found online in the Supporting Information section at the end of the article.